

NACA RM L55F02a



RESEARCH MEMORANDUM

A TRANSONIC WIND-TUNNEL INVESTIGATION OF THE STATIC
LONGITUDINAL CHARACTERISTICS OF A 3-PERCENT-THICK,
ASPECT-RATIO-3, DELTA WING CAMBERED AND TWISTED
FOR HIGH LIFT-DRAG RATIOS

By Dale L. Burrows and Warren A. Tucker

~~CONFIDENTIAL~~
Langley Aeronautical Laboratory
UNCLASSIFIED Langley Field, Va.

To _____
By authority of NACA Res abs Date effective
YRV-128 June 24, 1958
Am 9-8-58 6

CLASSIFIED DOCUMENT

This material contains information affecting the National Defense of the United States within the meaning of the espionage laws, Title 18, U.S.C., Secs. 793 and 794, the transmission or revelation of which in any manner to an unauthorized person is prohibited by law.

NATIONAL ADVISORY COMMITTEE FOR AERONAUTICS

WASHINGTON

August 5, 1955

RECEIVED COPY

AUG 11 1955

RECEIVED
AUG 11 1955
LANGLEY FIELD, VIRGINIA

NATIONAL ADVISORY COMMITTEE FOR AERONAUTICS

RESEARCH MEMORANDUM

A TRANSONIC WIND-TUNNEL INVESTIGATION OF THE STATIC
LONGITUDINAL CHARACTERISTICS OF A 3-PERCENT-THICK,
ASPECT-RATIO-3, DELTA WING CAMBERED AND TWISTED
FOR HIGH LIFT-DRAG RATIOS

By Dale L. Burrows and Warren A. Tucker

SUMMARY

A wind-tunnel investigation was made for Mach numbers ranging from 0.77 to 1.39 of a 3-percent-thick, aspect-ratio-3, delta wing on a slender cylindrical body through the angle-of-attack range from 0° to 20° and for Reynolds numbers of about 5×10^6 . The wing was cambered and twisted for the purpose of obtaining low drags at lifting conditions. A Mach number of 1.2 and a lift coefficient of 0.2 were used as design conditions. Although the wing was designed for a supersonic Mach number, a rather high value of maximum lift-drag ratio of 16 was obtained in the high subsonic region. This value was 23 percent greater than the value measured with a plane wing of the same plan form and thickness distribution and corresponded closely to the value obtained by adding the theoretical minimum induced drag coefficient, $\frac{(\text{Lift coefficient})^2}{\pi(\text{Aspect ratio})}$, to the zero-lift drag coefficient of the plane wing. Near the design Mach number, the value of lift-drag ratio of 11.5 corresponded to an increase in this ratio of 21 percent of that for the plane wing. These comparisons are made for about equal conditions of untrimmed moment. The variation of the pitching-moment coefficient with lift coefficient at zero lift was about the same for both wings throughout the Mach number range; the cambered and twisted wing, however, had a somewhat more gradual change with Mach number. An effect of camber and twist was to provide an improvement in lift-curve slope over that of the plane wing throughout the Mach number range tested.

INTRODUCTION

The possibility of realizing improvements in the maximum lift-drag ratio at supersonic speeds by the use of wing camber and twist has



received considerable attention both theoretically (refs. 1 to 4, for example) and experimentally (refs. 5 to 7). Much of the emphasis leading to the use of camber and twist has been placed on the load distributions in an effort to produce a minimum induced drag at lifting conditions. It has been recognized (refs. 3 and 4) that, theoretically, the flat wing of triangular plan form with full leading-edge suction has an induced drag which is very near the theoretical minimum value for optimum elliptical loading. Because of the experimental impossibility of obtaining the infinite velocities required for full leading-edge suction on a thin flat wing, it would seem that the design of a wing should be such as to avoid the necessity for infinite velocities at the leading edge. This result can be accomplished by putting the leading edge at an ideal angle of attack at the desired total lift. Such a condition for a swept wing implies the use of camber and twist. To date, however, none of the experimental investigations has been aimed at achieving a minimum value of the drag at a given lift by the use of a contour which is at the ideal angle of attack at all points along the leading edge.

The contour for the present investigation has avoided the requirements of a leading-edge suction by specifying that the lifting pressure distribution shall be linear in the chordwise direction at all points along the span. The general design method is presented in reference 8 and is applied for the specific case of this investigation in the appendix. The results of reference 8 added stimulus to the present investigation in the theoretical finding, that, for a slender triangular wing cambered and twisted under the conditions of linear chordwise lifting pressure distribution, the drag due to lift was about half that of a wing the same plan form with no camber or twist if no leading-edge suction was assumed for the latter. This finding is of importance because the practical thin flat wing rarely obtains a high degree of leading-edge suction and, therefore, a given plan form could benefit appreciably by the use of an optimum camber and twist.

In addition to providing a means for obtaining the linear lifting pressure distribution, the method of reference 8 permits the spanwise and chordwise loadings to be specified. The spanwise loading is the spanwise distribution of the load per unit span and in the same sense the chordwise loading is the chordwise distribution of the load per unit chord. Of interest in connection with loading is the statement in reference 1 that, for a slender wing lying near the center of the Mach cone, the minimum value of the drag with a given lift and span is achieved when both the spanwise and the chordwise load distributions are elliptical. An extension of this idea is given in reference 3, in which it is pointed out that, for wings which are not slender with respect to the Mach cone, the optimum chordwise loading is no longer elliptic but should have a finite value of the load at the trailing edge.

These considerations of lifting pressure and load distributions were used in the design of a triangular wing of aspect ratio 3 and 3 percent-chord thickness for a Mach number of 1.2 and a lift coefficient of 0.2. The resulting cambered and twisted wing was tested on a cylindrical body of fineness ratio 9.63. The tests were made at Mach numbers from 0.77 to 1.39 at Reynolds numbers (based on the mean aerodynamic chord) of about 5×10^6 and through an angle-of-attack range from 0° to 20° . The longitudinal force and moment data are compared with results for the plane wing of reference 7.

SYMBOLS

$\frac{C_1}{C_L}, \frac{C_2}{C_L}, \frac{C_3}{C_L}, \frac{C_4}{C_L}$	loading constants in equation (1) of appendix
C_D	drag coefficient, $\frac{\text{Drag}}{qS}$
C_{D0}	zero-lift drag coefficient of plane wing
C_L	lift coefficient, $\frac{\text{Lift}}{qS}$
C_{Lopt}	lift coefficient at $(L/D)_{max}$
c_l	local lift coefficient based on chord, $\frac{\text{Lift per unit span}}{qc}$
c_l'	local lift coefficient based on local span, $\frac{\text{Lift per unit chord}}{qb'}$
C_m	pitching-moment coefficient, $\frac{\text{Pitching moment about } \bar{c}/4}{qS\bar{c}}$
L/D	lift-drag ratio
$(L/D)_{max}$	maximum value of lift-drag ratio
P	lifting pressure coefficient, $\Delta p/q$
A	aspect ratio of wing

b	total wing span
b'	local span of wing to leading edge
c	local chord of wing
c _r	root chord of wing
K	drag-due-to-lift factor $\frac{C_D - C_{D0}}{C_L^2}$
k	plan-form parameter, $\frac{m}{m_1}$
M	average free stream Mach number at model location
m	cotangent of sweepback angle of leading edge
m ₁	cotangent of sweepback angle of trailing edge
n = βm	
p	free-stream absolute static pressure
Δp	difference in static pressure on upper and lower surface
P _t	free-stream absolute stagnation pressure
q	free-stream dynamic pressure, $\frac{\gamma P M^2}{2}$
γ	ratio of specific heat, 1.4 for air
R	free-stream Reynolds number based on \bar{c}
S	total wing area
\bar{c}	wing mean aerodynamic chord, $\frac{2}{S} \int_0^{b/2} c^2 dy = \frac{2}{3} c_r \left(\frac{1 - \lambda^3}{1 - \lambda^2} \right)$
s	semispan, b/2
t	maximum wing thickness at a given spanwise station
x, y, z	rectangular coordinates with origin at wing apex

x'	distance in x-direction measured from leading edge of local chord
α	angle of attack for the fuselage center line
$\beta = \sqrt{M^2 - 1}$	
$\sigma = y/s$	
λ	taper ratio of wing plan form

MODEL

The configuration details of the model are shown in a sketch in figure 1. The wing was of delta plan form and had an aspect ratio of 3. The thickness distribution was the NACA 65A003 distribution superimposed on the cambered mean line in planes parallel to the plane of symmetry. This thickness distribution is the same as that for the plane wing of reference 7.

The photographs in figure 2 show the essential features of the wing contour. The ordinates of the mean-line surface were designed to give optimum lift-drag characteristics at a Mach number of 1.2 and a lift coefficient of 0.2. The ordinates were determined by the method given in the appendix and are presented in table I. The loadings used in the design method and other contour diagrams of more detail are shown in figures 3, 4, and 5.

The mean line surface was cambered and twisted and was distinct from the conical type of camber in that the only straight line on the surface was the trailing edge which allows a certain amount of convenience in attaching control surfaces. The trailing edge was made to pass through the body center line. The straight line presumably could have been placed at the control surface hinge line without altering the over-all aerodynamic characteristics of the wing.

The longitudinal position of the wing on the body is shown in figure 1 and is the same as that of the plane wing of reference 7. Both the wing and the body were made of steel. The body of fineness ratio 9.63 had an ogive (circular arc) nose of 3.5 body diameters in length and the rest of the body was cylindrical. The cylindrical part of the body was a hollow shell which housed the sting and strain-gage balance. The angle of incidence of the wing with respect to the body was determined (from the design method described in the appendix) to give zero lift when the body was at zero angle of attack.

APPARATUS AND METHODS

Tunnel

The tests were conducted in the Langley transonic blowdown tunnel in which Mach numbers up to 1.4 can be attained. At a given Mach number, the Reynolds number can be varied from approximately 8×10^6 to 24×10^6 per foot of chord by varying the stagnation pressure from 25 pounds per square inch absolute to 70 pounds per square inch absolute. The Mach number distribution in the longitudinal direction at the model location was constant within ± 0.01 ; the tunnel calibration of the Mach number distribution is presented in reference 7.

Tests

The investigation covered a Mach number range from 0.77 to 1.39 at angles of attack from about 0° to 12° for a pressure of 70 pounds per square inch, absolute and from 10° to 20° at 35 pounds per square inch, absolute. For a Mach number of 1.39, data were obtained at a stagnation pressure of 50 pounds per square inch, absolute at angles of attack of about 0° to 12° . The limits of angle of attack were dictated by balance-load limitations or by the angle-of-attack mechanism. Reynolds numbers based on \bar{c} for the various stagnation pressures are shown in figure 6. For all tests, the surface of the model was in a smooth condition. Shock reflections from the tunnel wall intersected the model at Mach numbers between about 1.04 and 1.10. Inasmuch as this condition may have introduced appreciable tunnel-wall effects on the force and moment data, no such data are presented in this Mach number range.

Measurements

The model was attached to an internal three-component strain-gage balance, which in turn was attached to a sting. (See fig. 1.) A small pressure tube extended inside the base of the body for the purpose of recording base pressures. Normal-force, chord-force, pitching-moment, and base-pressure data were recorded simultaneously on film. The chord-force coefficient was adjusted to a condition of base pressure equal to free-stream static pressure. Normal-force and chord-force coefficients were converted to lift and drag coefficients by the usual methods. Mach numbers shown with the data are accurate to about ± 0.01 and angles of attack are accurate to about $\pm 0.1^\circ$.

Corrections

Reference 9 shows that, for slotted tunnels where the ratio of model size to tunnel size is about that of the present investigation, the jet-boundary effects are negligible; therefore, no such correction has been

made to the data. Angle of attack was corrected for sting and balance deflection resulting from aerodynamic load.

A loading test to determine the effects of elasticity on the plane wing of the same thickness and plan form as the present wing (ref. 7) indicated that aeroelasticity might have produced a maximum decrease in lift-curve slope of the order of 2 percent and a forward shift in aerodynamic-center position of about 0.01c. Although the camber and twist affords an added rigidity, this effect is probably offset by the increased loading of the tip and hence the present wing might be expected to have a similar degree of aeroelastic effects as the plane wing. In the data presented, no correction for aeroelasticity has been applied.

RESULTS AND DISCUSSION

An index of the figures presenting the results of this investigation follows:

	<u>Figure</u>
C_L against α	7
$\left(\frac{dC_L}{d\alpha}\right)_{C_L=0}$ against M	8
C_D against C_L	9
C_D against M (at constant lift)	10
L/D against C_L	11
$(L/D)_{max}$ and C_{Lopt} against M	12
C_L against C_m	13
$\left(\frac{dC_m}{dC_L}\right)_{C_L=0}$ against M	14

Throughout the discussion of the results of this investigation, comparisons are made between the measured results for the cambered and twisted wing and the measured results for the plane wing of the same plan form and thickness distribution reported in reference 7. The theoretical drag due to lift characteristics for the cambered and twisted wing is of interest throughout the Mach number range but has not been generally determined because of the great complication in making the calculations for other than the design condition. As indicated in references 3 and 4, however, the theoretical full leading-edge suction induced-drag predictions for plane triangular wings would be close to the optimum and, therefore, would seem useful as a basis of comparison with the measured results of the cambered and twisted wing.

Lift characteristics.- The basic data of lift coefficient plotted against angle of attack is shown in figure 7. At all Mach numbers tested, the variation of lift was nearly linear with angle of attack up to lift coefficients of about 0.4. There was only a slight rounding off of lift coefficients with angle of attack up to lift coefficients of 0.9. The angle of attack for zero lift is seen to be about 1.2° for Mach numbers up to about unity and drops to about 0.85° for low supersonic Mach numbers. (Also see plot in figure 8.) The case of zero lift at positive angle is, of course, equivalent to negative incidence although the model was designed for zero incidence. Whether this amount of incidence is desirable from a consideration of optimum lift-drag ratio is not known.

The values of the lift-curve slope at zero lift are shown in figure 8 where it may be seen that the usual characteristic increase in $C_{L\alpha}$ with Mach number occurs in the subsonic range. The value of $C_{L\alpha}$ increases from 0.056 at $M = 0.76$ to 0.072 at $M = 0.98$ and returns to a value of 0.056 at $M = 1.3$. The slope of the lift curve for the cambered and twisted wing is about 8 percent higher than for the plane wing in the subsonic range and about 4 percent higher in the supersonic range.

The theoretical lift-curve slopes presented in figure 8 for the plane wing-body combination were determined by the method of reference 10. This method required the wing-alone lift-curve slopes which were obtained from the theories of DeYoung and Harper (ref. 11) and Brown (ref. 12) for the subsonic and supersonic speed range, respectively. In the subsonic range $C_{L\alpha}$ for the cambered and twisted wing falls on or near the theoretical value for the plane wing (fig. 8). This result suggests that the cambered and twisted wing had a negligible amount of separated flow. In the supersonic range, $C_{L\alpha}$ for the cambered and twisted wing was only slightly closer to plane-wing theory than the plane-wing results. The reason for the improvement being so slight is not apparent.

Drag characteristics.- The basic drag results are plotted as drag coefficient against lift coefficient in figure 9. Cross plots of drag coefficient against Mach number are shown in figure 10 for lift coefficients of 0.1, 0.2, 0.3, 0.4, 0.5, and the lift coefficient corresponding to minimum drag coefficient. The effect of camber and twist is to make the minimum drag occur at a lift coefficient of about 0.1 in the subsonic range. In the supersonic range, the value of the lift coefficient for minimum drag decreased with increasing Mach number, probably because of loss of camber benefits as the Mach cone approached the leading edge.

The minimum drag coefficient for the cambered and twisted wing has about 0.01 for Mach numbers between 0.77 and 0.94 and reached a value of about 0.018 at a Mach number of about 1.10. At higher Mach numbers, the

minimum drag coefficient drops slightly to 0.017 at $M = 1.39$. These values of the minimum drag coefficient are about 10- to 30-percent higher than those for the plane wing through the Mach number range up to the design Mach number. At the design Mach number the increase was about 10 percent.

The minimum drag coefficient is shown to approach the plane-wing value as closely at the design Mach number (1.2) as at subsonic speeds. On either side of this Mach number, however, the drag rises rapidly, which suggests that the camber acts similarly to additional thickness at Mach numbers higher than the design Mach number; whereas, at Mach numbers below the design value, the increases in drag probably result from a carry-over of the usual transonic drag-rise effects. The transonic rise in minimum drag coefficient for the cambered and twisted wing was about 0.0080, which is somewhat higher than the value of 0.0066 for the plane wing. Both wings, however, have about the same percentage (75 percent) of drag rise through the transonic range.

At higher lift coefficients, such as 0.3 and 0.5 shown in figure 10, the drag coefficient of the cambered and twisted wing is appreciably lower in the high subsonic Mach number range than that of the plane wing. For example, at a Mach number of 0.98 and a lift coefficient of 0.5, the drag coefficient of the cambered and twisted wing is 25 percent lower than that of the plane wing at the same condition. The difference in drags at high lift would appear to be of considerable interest in connection with performance in high-speed maneuvers. The cambered and twisted wing also shows gains in drag at higher lifts at supersonic speeds especially at the design Mach number (1.2).

Values of the lift-drag ratios are plotted against lift coefficient in figure 11 and were used to obtain the maximum values of lift-drag ratio that are shown in figure 12 plotted against Mach number. In addition, values of the lift coefficient at maximum lift-drag ratio ($C_{L_{opt}}$) are shown in figure 12. Although the cambered and twisted wing was designed for a supersonic Mach number, large gains were obtained in values of the maximum lift-drag ratio at subsonic speeds over those of the plane wing. At a Mach number of 0.95, for example, the maximum lift-drag ratio for the cambered and twisted wing was 16 as compared with 13 for the plane wing, so that a gain of 23 percent was realized. This gain is appreciable as compared with the gain of 5 percent for the cambered (no twist) wing of reference 7.

The theoretical values of maximum lift-drag ratio presented in figure 12 were obtained from the relation $\frac{1}{2\sqrt{KC_{D_0}}}$. For full leading-edge suction, the drag-due-to-lift factor K for subsonic speeds was taken

as $\frac{1}{\pi A}$ and for supersonic speeds was obtained from reference 12. The values of K for zero leading-edge suction were taken as $\frac{1}{57.3 \left(\frac{dC_L}{d\alpha} \right)_{C_L=0}}$, where the theoretical value of $\left(\frac{dC_L}{d\alpha} \right)_{C_L=0}$ was obtained from figure 8.

At subsonic speeds up to a Mach number of 0.95, the cambered and twisted wing gave values of maximum lift-drag ratio that were about equal to the calculated values for the plane wing. A comparison of calculated and measured drag coefficients plotted against lift coefficient are shown in figure 15 for several representative Mach numbers. The calculated drags were determined by adding the theoretical value of the drag due to lift with full suction to the minimum experimental drag of the plane wing of the same plan form and thickness distribution (ref. 7). The measured drags are about equal to the calculated drags for lift coefficients between approximately 0.1 and 0.3 for Mach numbers up to 0.95. This result led to the conclusion that the profile drag of the cambered and twisted wing at optimum lift was equal to the profile drag of the plane wing at zero lift and the induced drag was equal to the theoretical minimum $C_L^2/\pi A$ (except for very low aspect ratio effects as discussed in reference 13). This conclusion must result because the profile drag of the cambered and twisted wing at any lift would not be expected to be less than the profile drag of the plane wing at zero lift and the induced drag cannot be less than the theoretical value. The possibility that the profile drag of the cambered and twisted wing at the optimum lift could be as low as the zero-lift profile drag of the plane wing is entirely reasonable because of the low loading at the leading edge which is near the ideal angle of attack. In addition it is of interest to note that, since part of the total drag is equal to $\frac{C_L^2}{\pi A}$ (the theoretical potential flow minimum), this part of the measured drag cannot be reduced by changes in Reynolds number. The value of the maximum lift-drag ratio, however, can be changed by Reynolds number but only through its effect on profile drag.

At supersonic Mach numbers, the variation in maximum lift-drag ratio with Mach number is somewhat unusual (fig. 12). At the design condition ($M = 1.2$), the cambered and twisted wing had a value of the maximum lift-drag ratio of 11.5 which is 13 percent higher than predicted by theory for the plane wing and 21 percent higher than measured on the plane wing. At supersonic Mach numbers on both sides of the design condition, the value of maximum lift-drag ratio dropped off markedly which suggests that the cambered and twisted wing is sensitive to Mach number. This result suggests that the optimum configuration of camber and twist should be quite different for each supersonic Mach number. On the other hand, it is possible that no configuration would have values of maximum lift-drag

ratio in the Mach number range from 1.0 to 1.1 much higher than are obtained by the plane wing of reference 7, as suggested by the result that the cambered wing (no twist) of reference 7 as well as the present wing affords very little improvement over the plane wing; this possibility is further indicated by the fact that the present cambered and twisted wing performs especially well both at a Mach number of 0.95 and 1.2 - that is, on both sides of the low transonic region. The reduction of maximum lift-drag ratios at Mach numbers somewhat higher than the design conditions could easily come about because of the increased profile drag (possibly separation) at lifting conditions and possibly reduced forward thrust at the off-design condition as the Mach cone approaches the leading edge.

The fact that the maximum lift-drag ratio is higher than the theoretical value for the plane wing at the design Mach number (1.2) is believed to be due in part to favorable effects of upwash produced by the body-wing combination and low-aspect-ratio effects which were not taken into account in the theory. Furthermore the theoretical method of determining the effect of the approach of the Mach cone to the leading edge on the possible amount of leading-edge suction may be somewhat inexact. In any case it can be shown that the measured values of lift-drag ratio are appreciably less than the values that would be obtained by using the minimum induced drag corresponding to $C_L^2/\pi A$ (which does not include any estimates of Mach cone compressibility effects). The fact that the experimental lift-drag ratios are higher than predicted by the particular supersonic theory used merely means, in part at least, that the results indicated a smaller degree of compressibility effects than would be predicted by theory.

Pitching-moment characteristics. - The basic pitching-moment data are presented in figure 13 as a function of lift coefficient. In general, it may be observed by comparisons with the results of reference 7 that the variation of pitching-moment coefficient with lift coefficient for the cambered and twisted wing is about as irregular (possibly slightly more so) than for the plane wing at all Mach numbers tested. The trim condition for the cambered and twisted wing occurred at a positive lift coefficient of about 0.05 and hence the cambered and twisted wing requires less trim (and thus less trim drag) than would be required by the plane wing at low lift coefficients. In the untrimmed condition, however, comparison of both wings at low lifts showed that the cambered and twisted wing had a higher drag than the plane wing. The relative merits of the two wings from consideration of drag at trimmed conditions and low lift is not obvious. The values of the pitching-moment coefficient at the optimum lift coefficient, however, are seen in figure 16 to be about the same for both wings throughout the Mach number range and, therefore, the relative gains in maximum lift-drag ratio indicated in figure 12 are indicative of the relative merits of the two wings in the trim condition.

The slope of pitching-moment coefficient against lift coefficient at zero lift shown in figure 14 indicates that the cambered and twisted wing has about the same aerodynamic-center position as the plane wing throughout the Mach number range. The cambered and twisted wing appears to provide some advantage over the plane wing in that the aerodynamic-center shift through the Mach number range is more gradual. Trends with Mach number agree with theory, but theoretical values of the aerodynamic-center position are somewhat (as much as 0.04c) rearward of the experimental values. The theoretical values of aerodynamic center for the plane wing-body combination were determined by the method of reference 10. This method required the wing-alone lift-curve slopes, which were obtained from references 11 and 12, and the wing-alone centers of pressure, which were obtained from reference 14.

CONCLUSIONS

Transonic wind-tunnel tests at Mach numbers from 0.77 to 1.39 on a 3-percent-thick, aspect-ratio-3, delta wing cambered and twisted for optimum lift-drag ratios at a design Mach number of 1.2 and a lift coefficient of 0.2 has resulted in the following conclusions and comparisons with a plane wing of the same plan form and thickness distribution:

1. The cambered and twisted wing when compared to the plane wing showed an increase in the lift-curve slope throughout the Mach number range.
2. The minimum values of the drag coefficient were about 10 to 30 percent higher for the cambered and twisted wing than for the plane wing through the Mach number range up to the design Mach number; at moderate and high lift coefficients up to the design Mach number, the cambered and twisted wing showed appreciable drag reductions as compared with the plane wing.
3. The cambered and twisted wing produced large gains in maximum lift-drag ratio in comparison with values for the plane wing and reached values of this ratio of 16 near a Mach number of 0.95, which corresponded closely to the theoretical minimum induced drag and amounted to a 23 percent gain as compared with the plane-wing results. Near the design Mach number, the camber and twist produced values of the maximum lift-drag ratio (11.5) which exceeded the values obtained by the particular plane-wing theory used by 13 percent and the measured plane-wing results by 21 percent.
4. The cambered and twisted wing appeared to be sensitive to Mach number in the supersonic range, inasmuch as the maximum lift-drag ratio dropped off rather sharply above and below the design Mach number.

5. At the lift coefficients corresponding to maximum lift-drag ratio, the cambered and twisted wing and the plane wing had about equal values of the pitching-moment coefficient through the Mach number range.

6. The aerodynamic centers of both wings were very nearly the same; however, within the small differences noted, the cambered and twisted wing had a slightly more gradual shift of aerodynamic center with Mach number than the plane wing.

Langley Aeronautical Laboratory,
National Advisory Committee for Aeronautics,
Langley Field, Va., May 24, 1955.

APPENDIX A

DESIGN PROCEDURE FOR TWISTED AND CAMBERED WING

General Method

In the calculation of the desired twist and camber of the wing, no attempt was made to account for the presence of the body. The wing was treated as if it extended to the center line of the body, and the body was regarded as nonexistent. The general design procedure made use of the method of reference 8 to determine the ordinates of a zero-thickness wing that would have the desired chordwise distribution of lifting pressure and the desired load distribution (approximately elliptic in both the spanwise and the chordwise directions). The method essentially involves the use of generalized tables that give the ordinates of the mean-line surface as a function of the Mach number, wing-plan-form geometry, load distribution, and lift. The wing ordinates were next modified by shearing the spanwise stations vertically (without changing the local angle at any station) so that the wing trailing edge became a straight line. This modification to the calculated ordinates, which should have little aerodynamic effect, was made in order to give a wing on which a trailing-edge control might easily be mounted. The desired thickness distribution (that of the NACA 65A003 airfoil section) was then superimposed on the zero-thickness wing. Finally, the wing was mounted on the body so that at the design Mach number ($M = 1.2$) the total lift of the configuration would be approximately zero when the body was at zero angle of attack.

Detailed Calculations

The lifting pressure coefficient described by equation (2) of reference 8 was used to obtain the load distribution:

$$\frac{P}{C_L} = \frac{C_1}{C_L} + \frac{1-k}{1-\lambda} \frac{C_2}{C_L} \frac{x}{c_r} + \frac{C_3}{C_L}(\sigma) + \frac{C_4}{C_L}(\sigma)^2 \quad (1)$$

The procedure followed in determining the constants is in most respects like that used in example IV of reference 8. Thus, the spanwise load distribution is given by equation 9 of reference 8,

$$\begin{aligned} \frac{cc_l}{c_r C_L} &= \left(\frac{C_1}{C_L} + \frac{1-k}{2} \frac{C_2}{C_L} \right) - \left(\frac{C_1}{C_L} - k \frac{C_2}{C_L} - \frac{C_3}{C_L} \right) \sigma - \\ &\quad \left(\frac{1+k}{2} \frac{C_2}{C_L} + \frac{C_3}{C_L} - \frac{C_4}{C_L} \right) \sigma^2 - \frac{C_4}{C_L} \sigma^3 \end{aligned} \quad (2)$$

and the values of the constants $\frac{C_1}{C_L}$, $\frac{C_2}{C_L}$, and $\frac{C_4}{C_L}$ may be expressed in terms of $\frac{C_3}{C_L}$ (equations (14) of reference 8):

$$\left. \begin{aligned} \frac{C_1}{C_L} &= \frac{C_3}{C_L} \\ \frac{C_2}{C_L} &= \frac{4}{\pi} - 2 \frac{C_3}{C_L} \\ \frac{C_4}{C_L} &= 6 - \frac{16}{\pi} \end{aligned} \right\} \quad (3)$$

Also, as for the example mentioned, the chordwise load distribution (in the same sense as spanwise load distribution) is given by the following equation:

$$\frac{b'c_l'}{bC_L} = \frac{C_3}{C_L} \frac{x}{c_r} + \left(\frac{4}{\pi} - 2 \frac{C_3}{C_L} \right) \left(\frac{x}{c_r} \right)^2 + \left(2 - \frac{16}{3\pi} \right) \left(\frac{x}{c_r} \right)^3 \quad (4)$$

(In reference 8, this quantity was designated as Local lift/Total lift.) For the present case, the load given by equation (4) is specified to be equal to 0.2 at the trailing edge ($x/c_r = 1$) rather than zero as in example IV of reference 8. This condition was imposed on the basis of the statement in reference 3 that for wings which are not slender with respect to the Mach cone, the optimum chordwise loading should not be elliptic, but should have a finite value at the trailing edge. No method was available for determining the optimum trailing-edge load, so a value of 0.2 was chosen arbitrarily. A calculated value of the drag for this trailing-edge load was lower than the calculated drag for the condition of zero load at the trailing edge so that the choice of 0.2 was an improvement, though probably not the optimum value.

The condition on the chordwise load at the trailing edge determines the value of $\frac{C_3}{C_L}$ from equation (4); the other constants can then be evaluated from equation (3). The final numerical values of the constants are as follows:

$$\left. \begin{aligned} \frac{C_1}{C_L} &= \frac{C_3}{C_L} = 2.7512 \\ \frac{C_2}{C_L} &= -4.2292 \\ \frac{C_4}{C_L} &= 0.9070 \end{aligned} \right\} \quad (5)$$

The chordwise and spanwise loadings corresponding to this set of constants is shown in figure 3. For comparative purposes, elliptic loadings are also shown in the figure.

The values of the constants from equation (5) can be used with table II of reference 8 to calculate the zero-thickness wing ordinates before shearing. The other quantities to be used in the table are as follows: $\lambda = K = 0$, $m = 0.7536$, $M = 1.2$, $n = 0.5$, $C_L = 0.2$ (the value of \bar{x}'/\bar{c} used in reference 8 for fixing the aerodynamic center is not used for this example). The calculations are straightforward and need no further explanation. A solution for the wing contour at the mid-span would result in an infinite angle of attack. This singular result is of course of no consequence due to the fact that a fuselage body will in most cases cover this portion of the wing.

The constants of equation (5) can be put in equation (1) to give the following equation for the distribution of lifting pressure coefficient:

$$\frac{P}{C_L} = 2.7512 (1 + \sigma) + 0.907\sigma^2 - 4.2292 \frac{x}{c_r} \quad (6)$$

Chordwise contours of the wing mean-line surface and the lifting pressure distribution are shown in figure 4 for the design condition. The contours have been sheared vertically to give a straight trailing edge, as mentioned in the preceding discussion. In order to give a clearer picture of the details, the chordwise contours are shown in percent of local chord and to an enlarged vertical scale in figure 5.

Ordinates for the mean line surface are presented in table I and the system of axes used is shown in figure 17. The x'/c axis is aligned with the free-stream velocity for the condition of $M = 1.2$ and $C_L = 0.2$. The body axis was placed at an angle of incidence of 2.92° with respect to the x'/c axis; this angle was determined by taking the theoretical value of $dC_L/d\alpha$ for the plane wing (0.0685 deg^{-1}) and converting to degrees at a lift coefficient of 0.2 in order to obtain approximately zero lift on the configuration when the body is at zero angle of attack.

REFERENCES

1. Jones, Robert T.: The Minimum Drag of Thin Wings in Frictionless Flow. Jour. Aero. Sci., vol. 18, no. 2, Feb. 1951, pp. 75-81.
2. Graham, E. W.: A Drag Reduction Method for Wings of Fixed Plan Form. Jour. Aero. Sci., vol. 19, no. 12, Dec. 1952, pp. 823-825.
3. Adams, Mac C. and Sears, W. R.: Slender-Body Theory - Review and Extension. Jour. Aero. Sci., vol. 20, no. 2, Feb. 1953, pp. 85-98.
4. Tsien, S. H.: The Supersonic Conical Wing of Minimum Drag. Ph.D. Thesis, Cornell Univ., June 1953.
5. Madden, Robert T.: Aerodynamic Study of a Wing-Fuselage Combination Employing a Wing Swept Back 63° . - Investigation at a Mach Number of 1.53 to Determine the Effects of Cambering and Twisting the Wing for Uniform Load at a Lift Coefficient of 0.25. NACA RM A9C07, 1949.
6. Hall, Charles F.: Lift, Drag, and Pitching Moment of Low-Aspect-Ratio Wings at Subsonic and Supersonic Speeds. NACA RM A53A30, 1953.
7. Burrows, Dale L. and Palmer, William E.: A Transonic Wind Tunnel Investigation of the Longitudinal Force and Moment Characteristics of a Plane and a Cambered Three-Percent-Thick Delta Wing of Aspect Ratio 3 on a Slender Body. NACA RM L54E25, 1954.
8. Tucker, Warren A.: A Method for the Design of Sweptback Wings Warped to Produce Specified Flight Characteristics at Supersonic Speeds. NACA RM L51F08, 1951.
9. Whitcomb, Charles F., and Osborne, Robert S.: An Experimental Investigation of Boundary Interference on Force and Moment Characteristics of Lifting Models in the Langley 16- and 8-Foot Transonic Tunnels. NACA RM L52L29, 1953.
10. Nielsen, Jack N., Kaattari, George E., and Anastasio, Robert F.: A Method for Calculating the Lift and Center of Pressure of Wing-Body-Tail Combinations at Subsonic, Transonic, and Supersonic Speeds. NACA RM A53G08, 1953.
11. DeYoung, John, and Harper, Charles W.: Theoretical Systematic Span Loading at Subsonic Speeds for Wings Having Arbitrary Plan Form. NACA Rep. 921, 1948.
12. Brown, Clinton E.: Theoretical Lift and Drag of Thin Triangular Wings at Supersonic Speeds. NACA Rep. 839, 1946. (Supersedes NACA TN 1183.)

13. Polhamus, Edward C.: A Note on the Drag Due to Lift of Rectangular Wings of Low Aspect Ratio. NACA TN 3324, 1955.
14. Lomax, Harvard, and Sluder, Loma: Chordwise and Compressibility Corrections to Slender-Wing Theory. NACA Rep. 1105, 1952. (Supersedes NACA TN 2295.)

TABLE I

MEAN-LINE PLANE FOR ASPECT-RATIO-3 DELTA WING CAMBERED AND TWISTED FOR ELLIPTICAL LOADING

x'/c	z/c								
	0.168	0.2	0.3	0.4	0.5	0.6	0.7	0.8	0.9
0	0.0619	0.0525	0.0368	0.0269	0.0189	0.0111	-0.0005	-0.0167	-0.0480
.005	.0627	.0532	.0376	.0279	.0197	.0118	.0004	-.0158	-.0467
.0075	.0630	.0535	.0380	.0281	.0200	.0121	.0008	-.0154	-.0461
.0125	.0634	.0539	.0385	.0288	.0207	.0216	.0016	-.0145	-.0452
.025	.0640	.0547	.0395	.0301	.0221	.0141	.0034	-.0123	-.0430
.050	.0642	.0554	.0407	.0315	.0241	.0164	.0060	-.0094	-.0392
.075	.0638	.0553	.0412	.0324	.0254	.0181	.0078	-.0068	-.0357
.1	.0629	.0547	.0414	.0330	.0263	.0194	.0095	-.0047	-.0322
.15	.0603	.0528	.0408	.0334	.0274	.0210	.0210	-.0015	-.0278
.2	.0569	.0502	.0395	.0330	.0276	.0219	.0136	+ .0012	-.0237
.25	.0529	.0469	.0376	.0321	.0272	.0222	.0147	.0034	-.0204
.3	.0486	.0433	.0354	.0306	.0266	.0221	.0153	.0051	-.0175
.35	.0441	.0396	.0328	.0288	.0256	.0216	.0155	.0062	-.0149
.4	.0397	.0358	.0300	.0268	.0243	.0209	.0153	.0068	-.0126
.45	.0352	.0318	.0272	.0247	.0227	.0199	.0149	.0072	-.0105
.5	.0307	.0279	.0242	.0225	.0209	.0188	.0143	.0074	-.0084
.55	.0263	.0241	.0213	.0201	.0190	.0175	.0135	.0074	-.0067
.6	.0222	.0205	.0183	.0177	.0170	.0159	.0125	.0072	-.0051
.65	.0183	.0170	.0156	.0152	.0149	.0142	.0113	.0068	-.0036
.7	.0146	.0137	.0129	.0128	.0128	.0123	.0101	.0063	-.0023
.75	.0111	.0106	.0103	.0104	.0107	.0103	.0088	.0056	-.0013
.8	.0081	.0079	.0079	.0080	.0085	.0083	.0073	.0047	-.0006
.85	.0055	.0055	.0056	.0057	.0063	.0062	.0056	.0037	-.0002
.9	.0032	.0033	.0034	.0036	.0042	.0041	.0038	.0026	0
.95	.0014	.0015	.0015	.0017	.0020	.0019	.0019	.0013	0
1.0	0	0	0	0	0	0	0	0	0

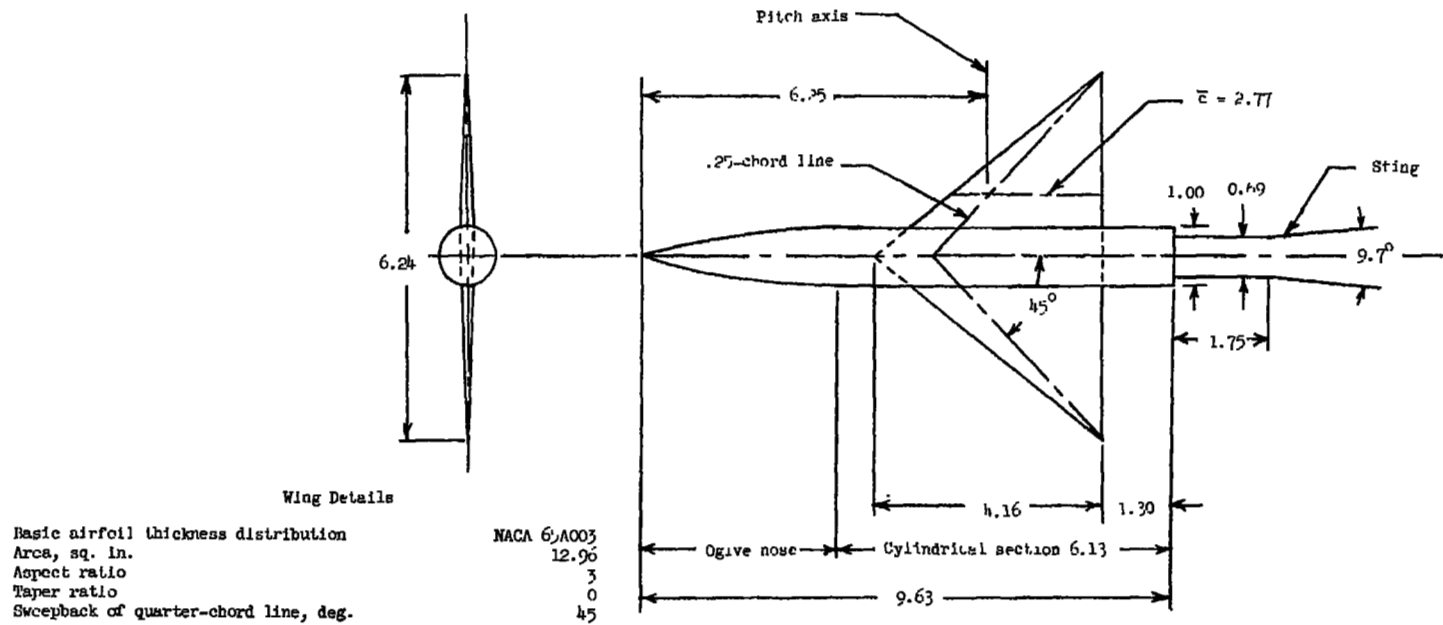
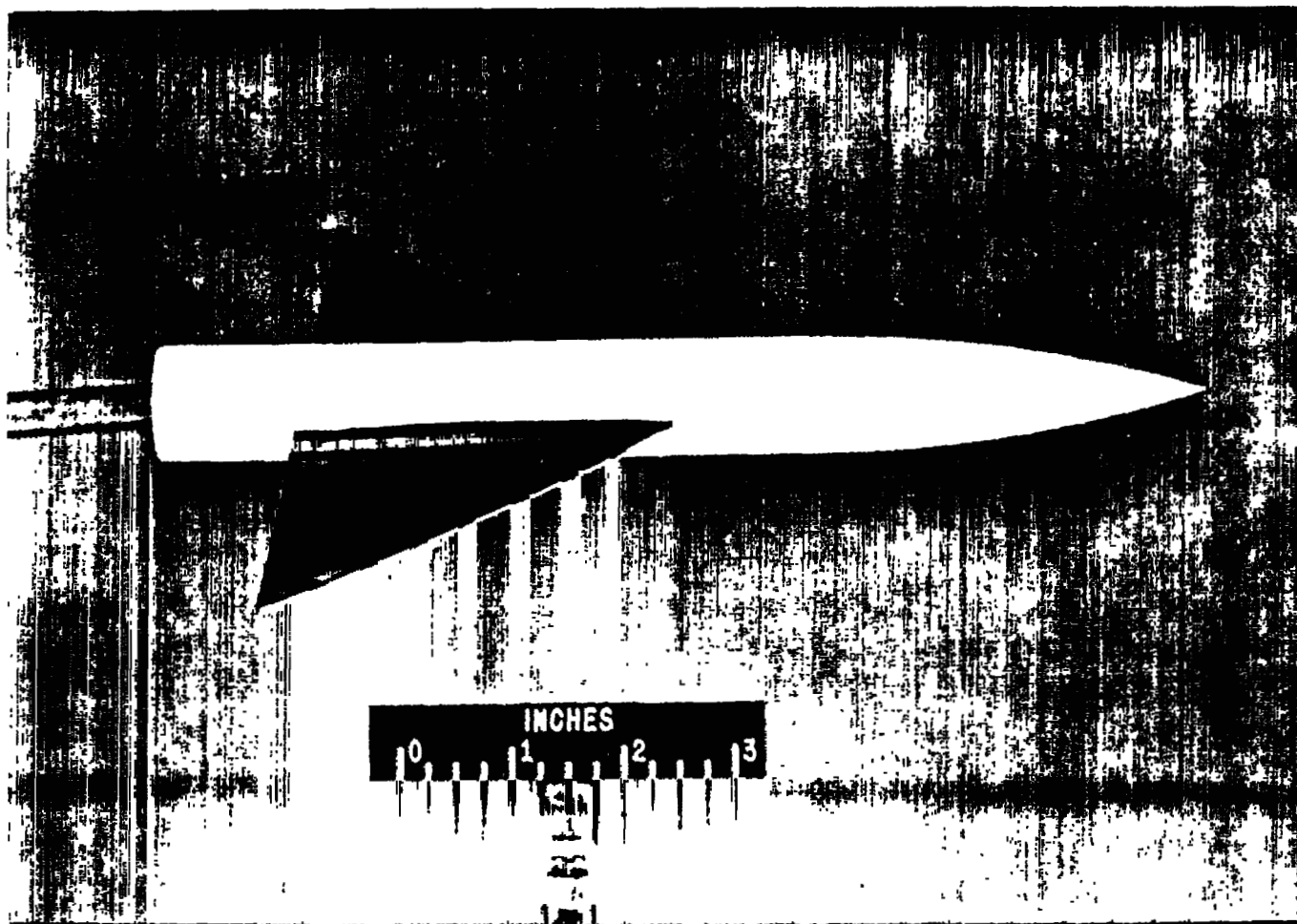


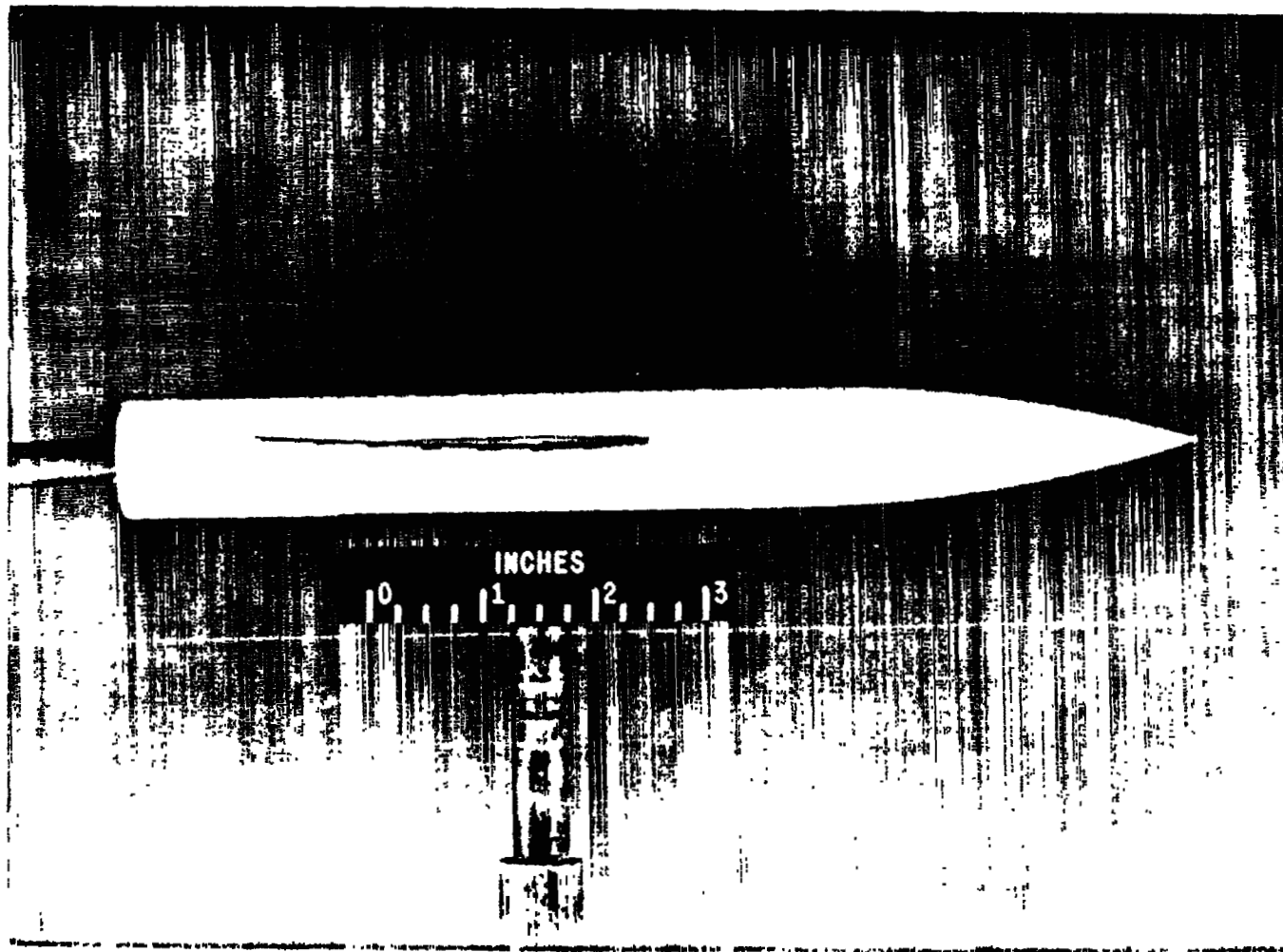
Figure 1.- Details of the wing-body configuration. All dimensions are in inches.



(a) Partial plan view.

L-87264

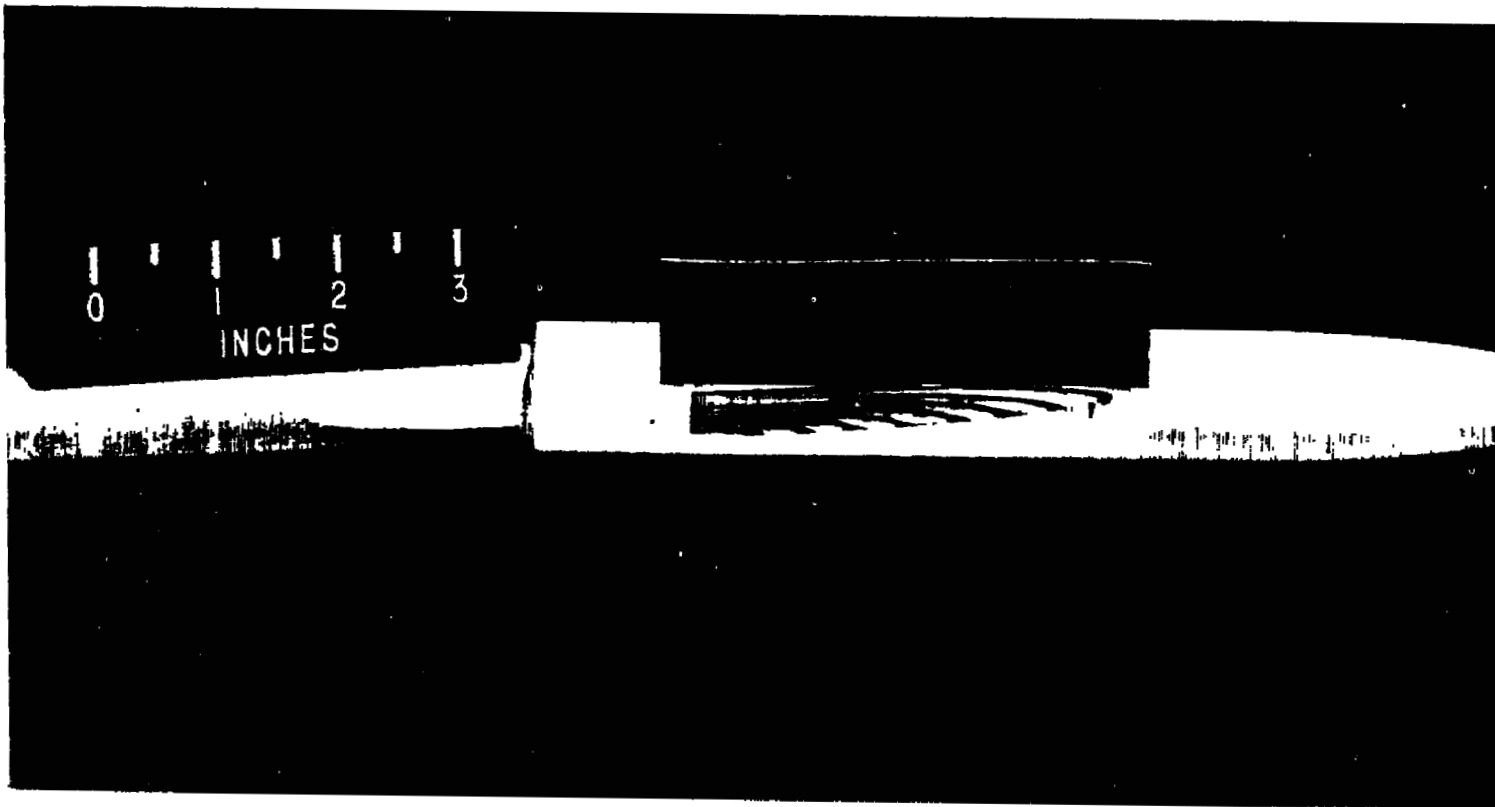
Figure 2.- Photographs of the model. Tape strips are parallel to plane of symmetry.



(b) Lower-surface end view.

L-87263

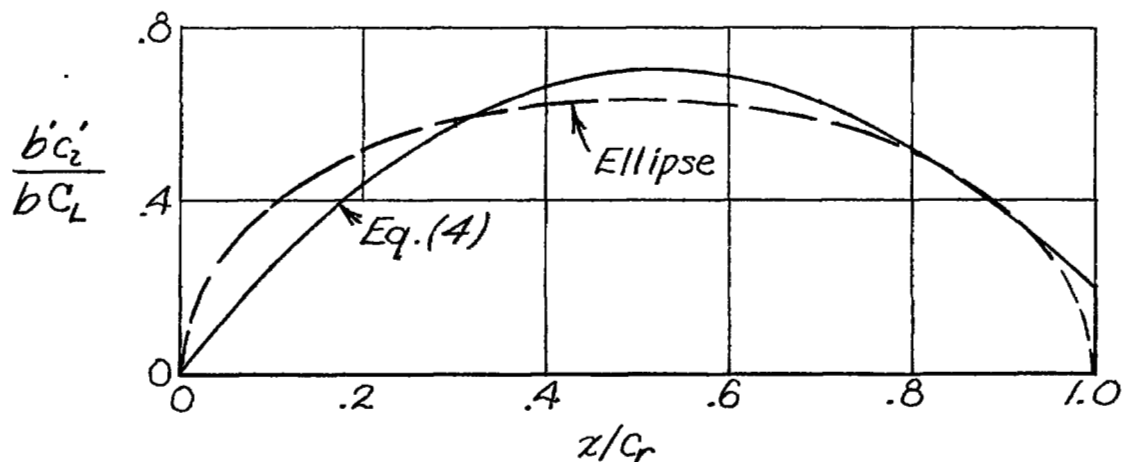
Figure 2.- Continued.



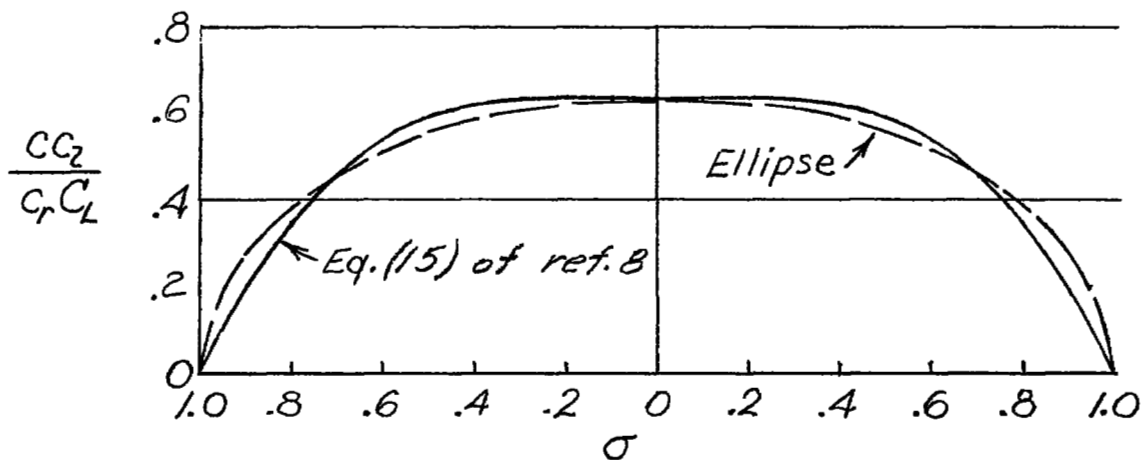
(c) Upper-surface end view.

L-87383

Figure 2.- Concluded.



(a) Chordwise loading.



(b) Spanwise loading.

Figure 3.- Calculated load distributions for twisted and cambered wing at design attitude.

~~CONFIDENTIAL~~

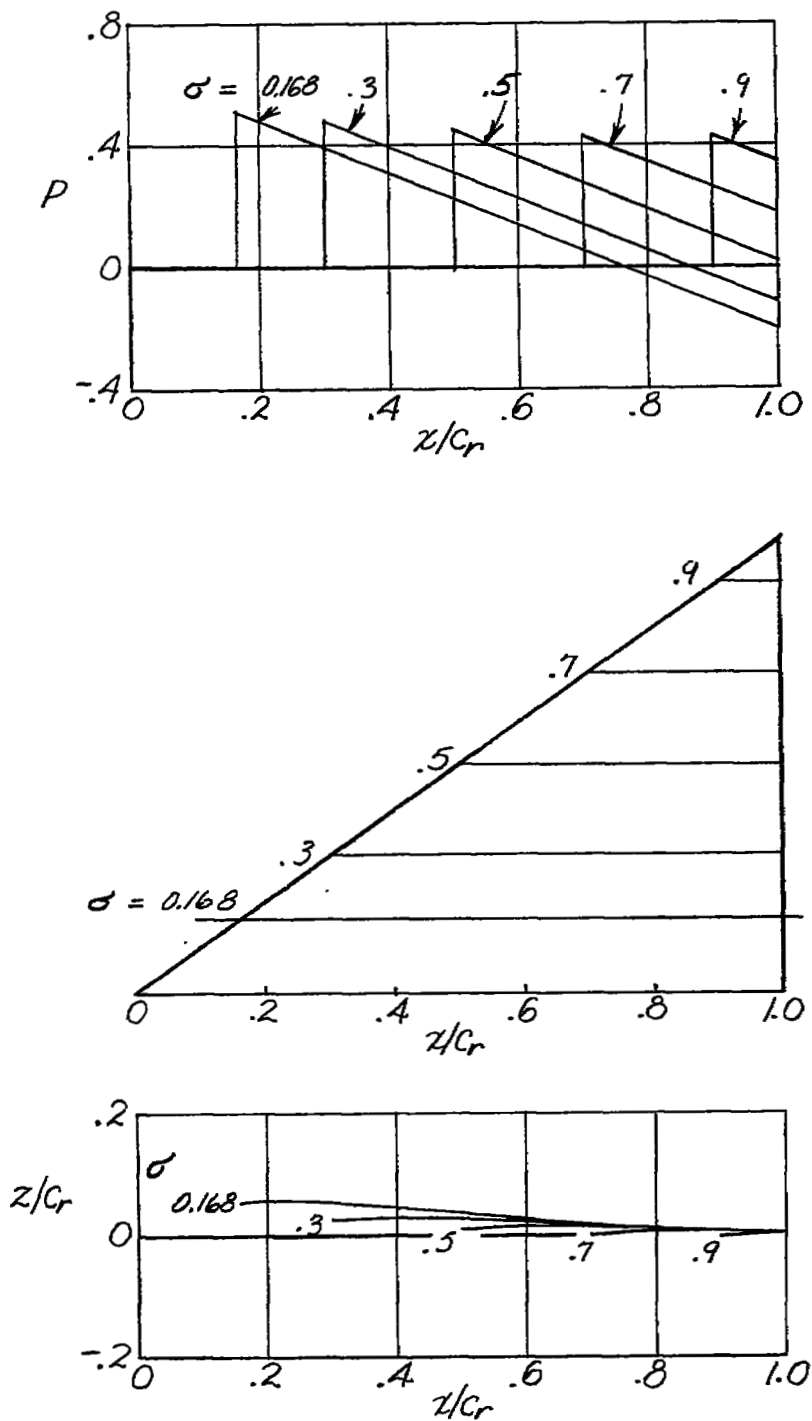


Figure 4.- Calculated shape and pressure distribution for twisted and cambered wing at design attitude. $M = 1.2$; $C_L = 0.2$; $\alpha = 2.92^\circ$.

~~CONFIDENTIAL~~

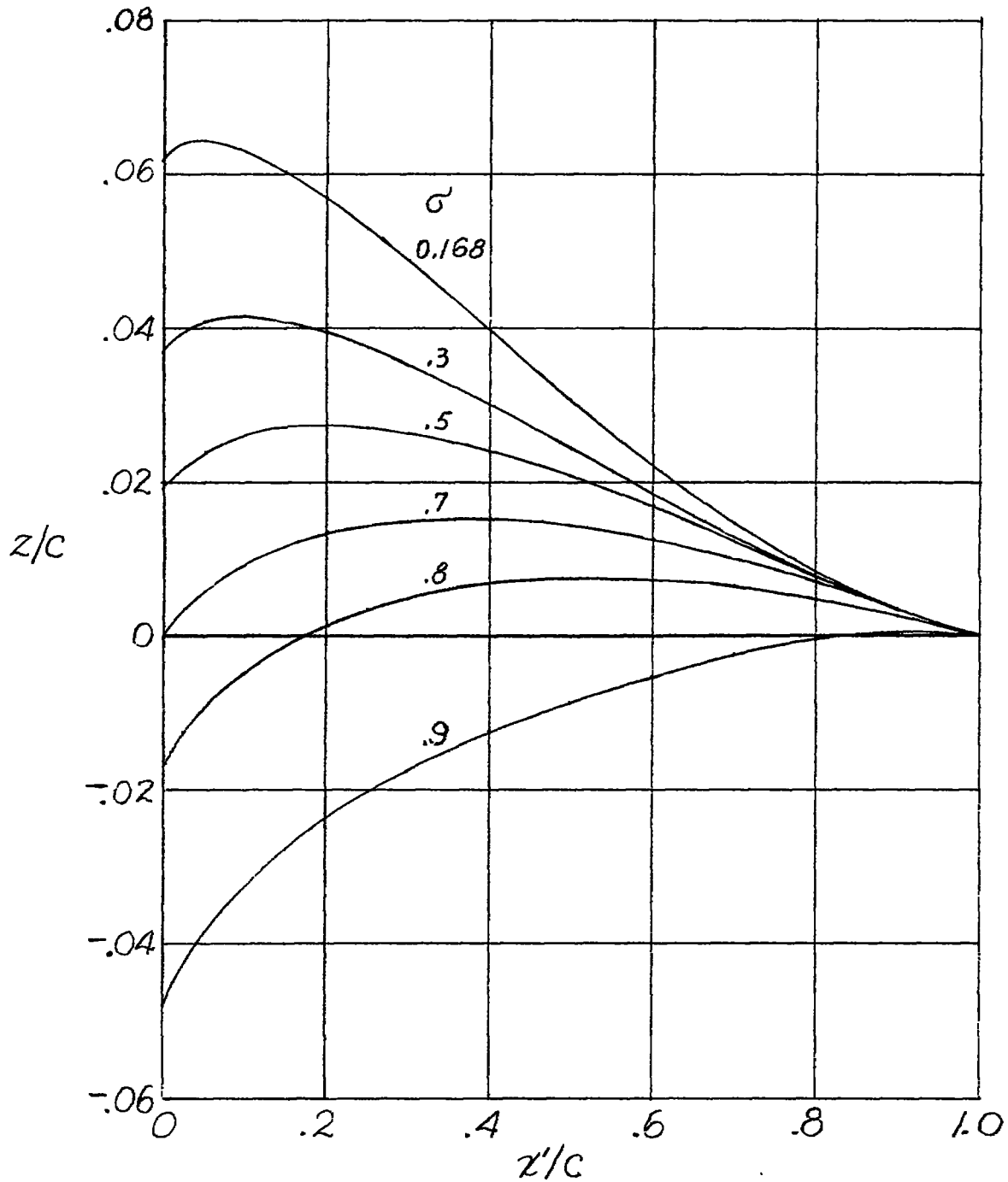


Figure 5.- Ordinates of twisted and cambered wing in terms of the local chord at $M = 1.2$, $C_L = 0.2$.

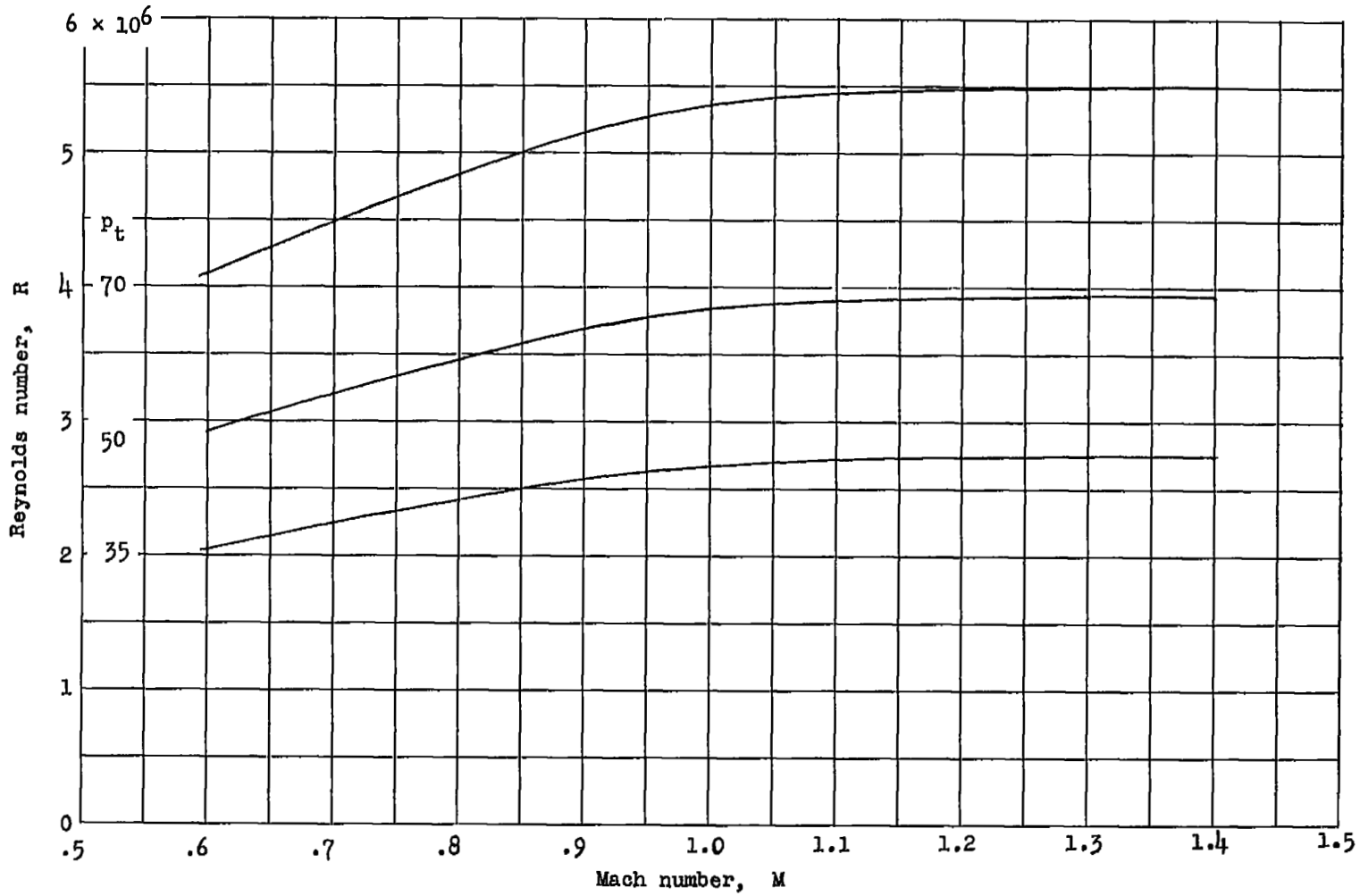


Figure 6.- Variation of Reynolds number with Mach number for stagnation pressures of 35, 50, and 70 pounds per square inch.

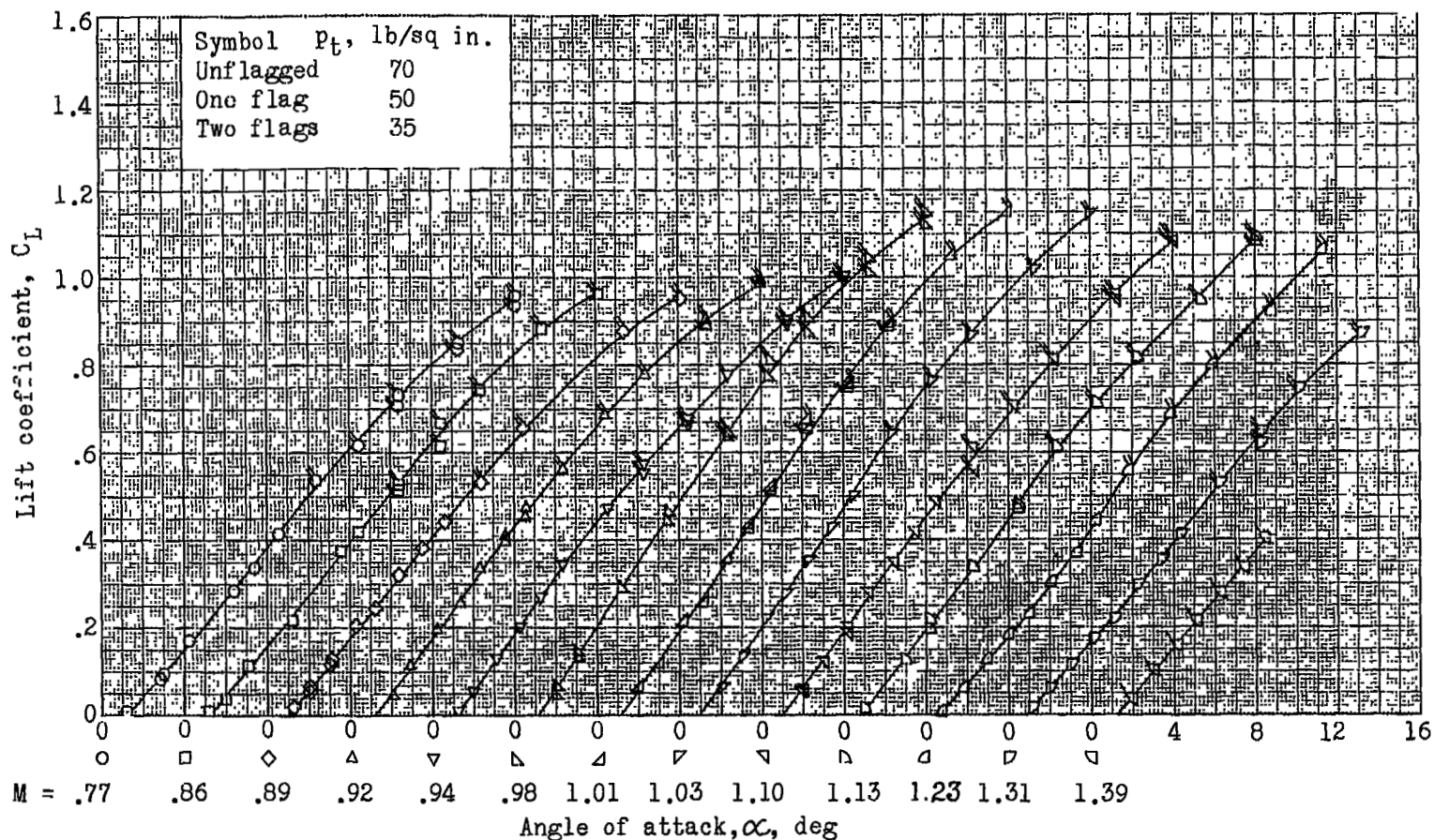


Figure 7.- Variation of lift coefficient with angle of attack at various Mach numbers for the wing-body combination. Cambered and twisted delta wing; $A = 3$; $t/c = 0.03$.

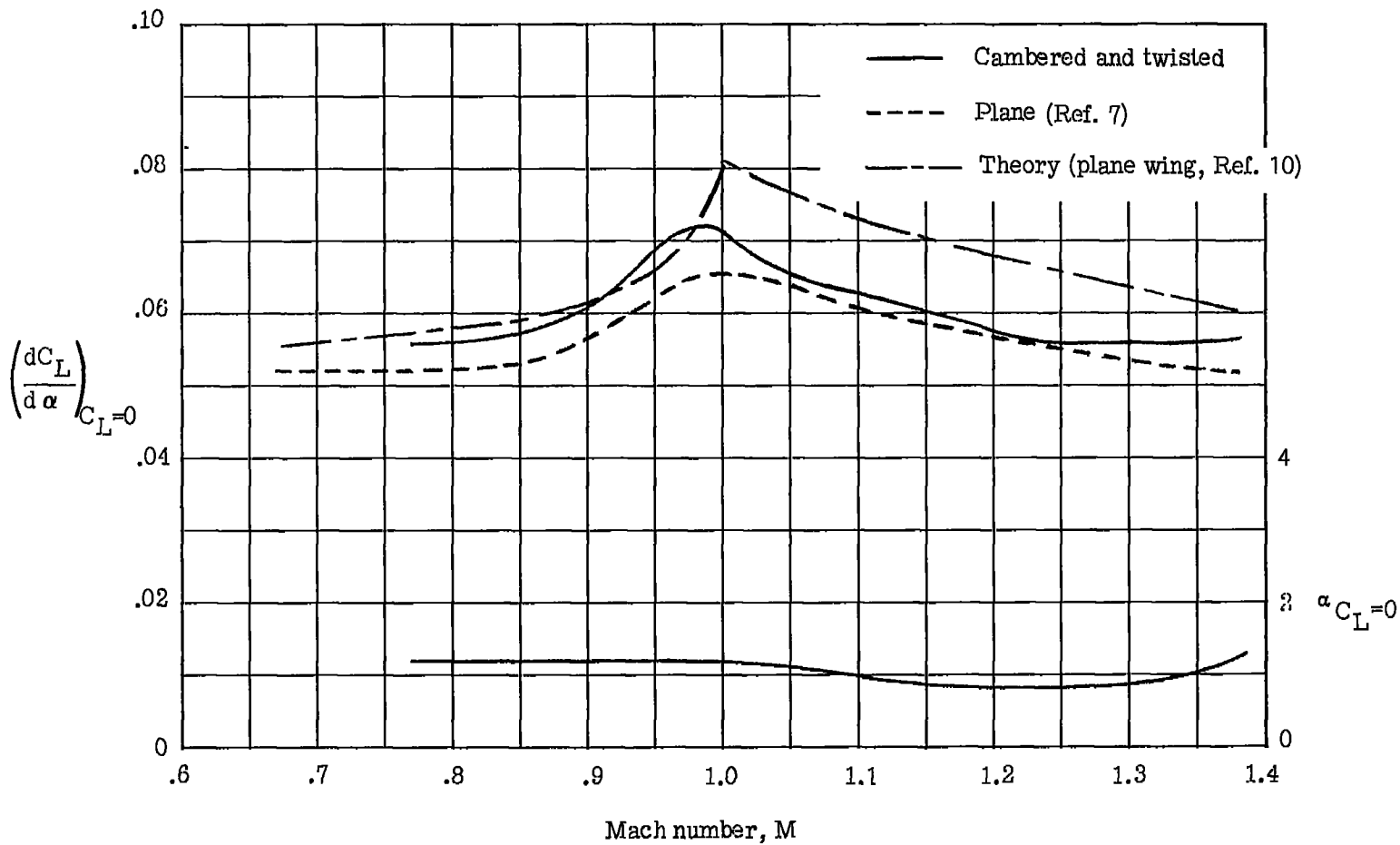


Figure 8.- Variation of lift-curve slope and angle of zero lift with Mach number for the wing-body combination. Delta wing; $A = 3$; $t/c = 0.03$.

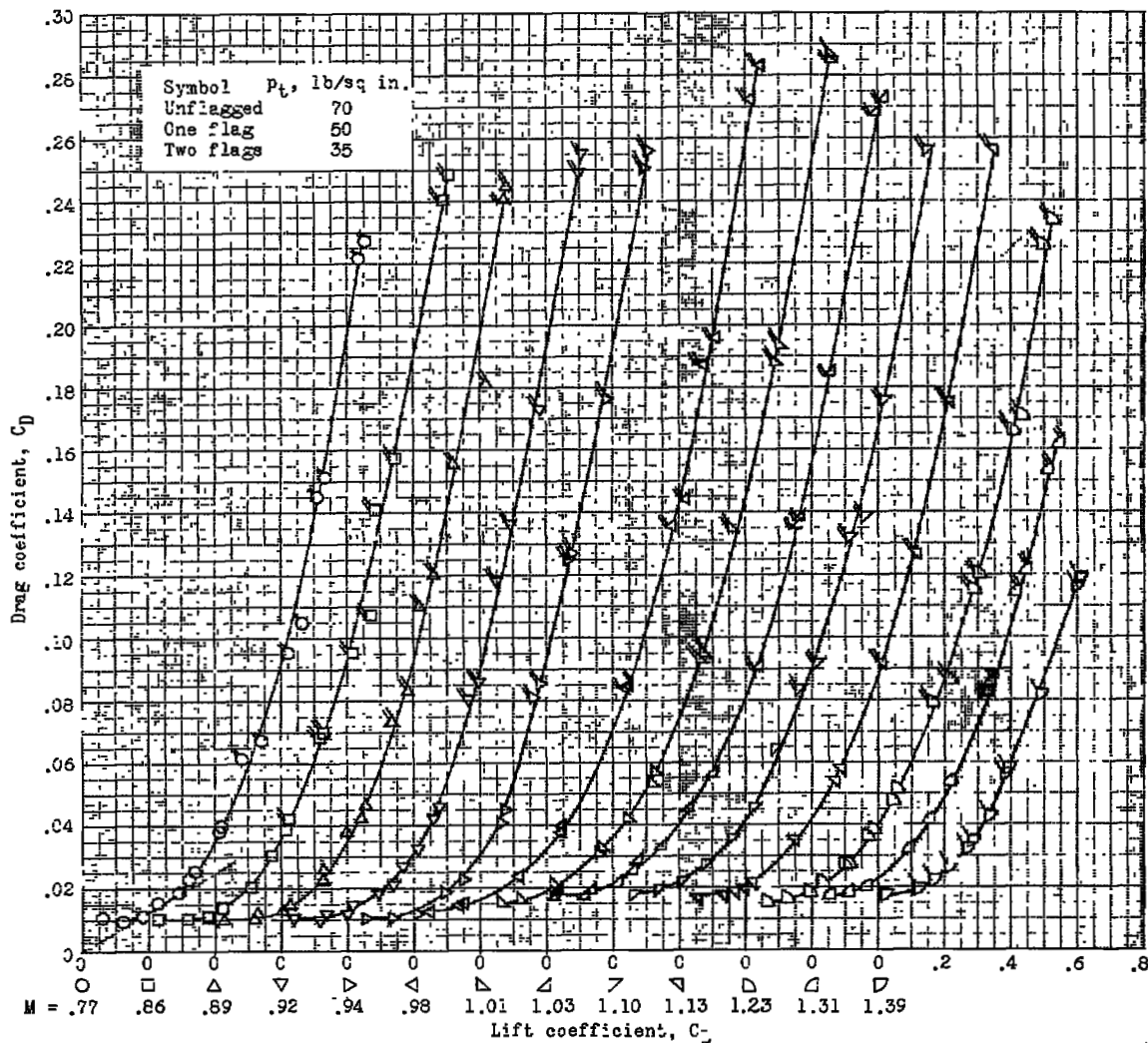


Figure 9.- Variation of drag coefficient with lift coefficient at various Mach numbers for the wing-body combination. Cambered and twisted delta wing; $A = 3$; $t/c = 0.03$.

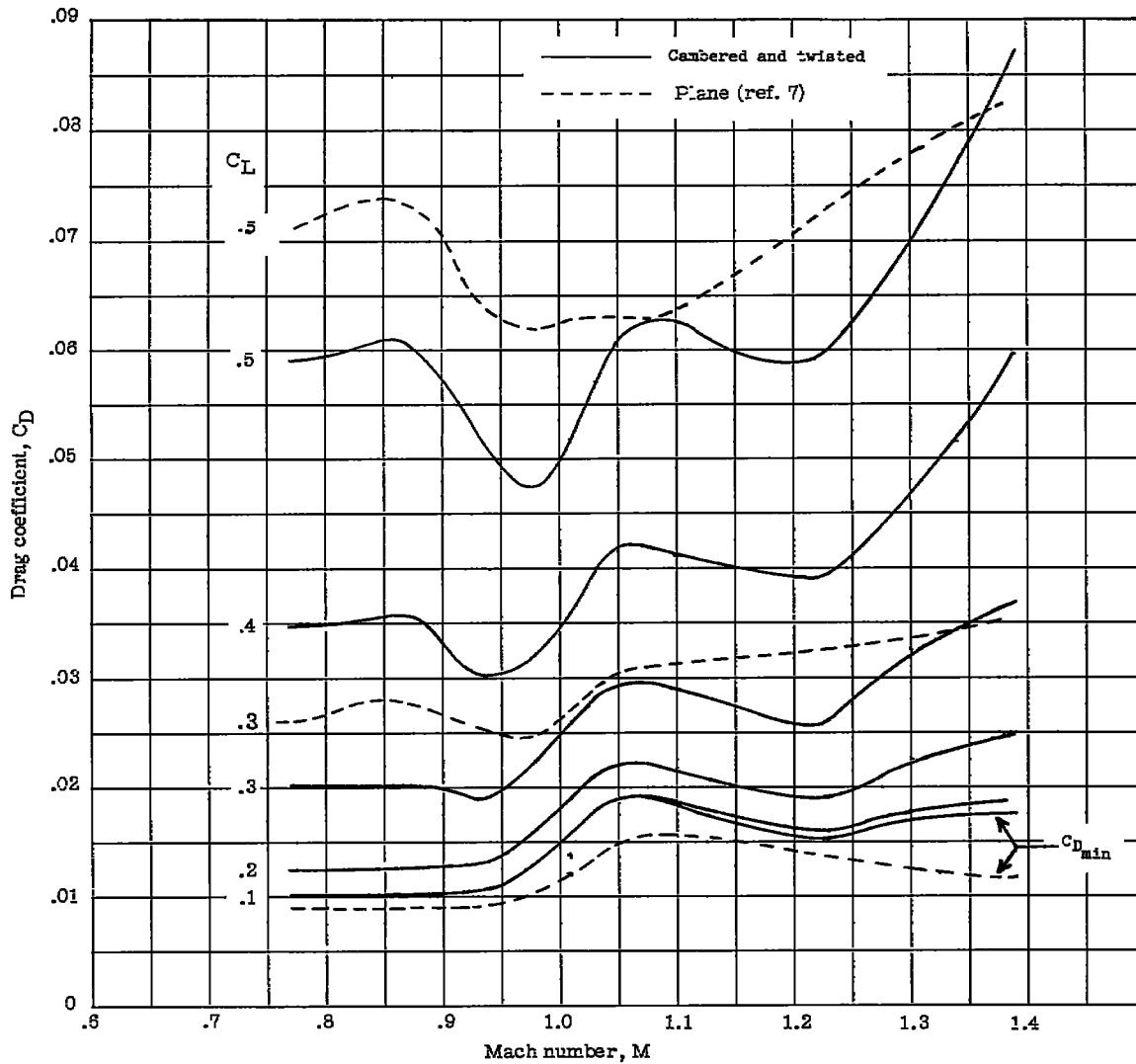


Figure 10.- Variation of drag coefficient with Mach number of various values of lift coefficient for the wing-body combination. Cambered and twisted delta wing; $A = 3$; $t/c = 0.03$.

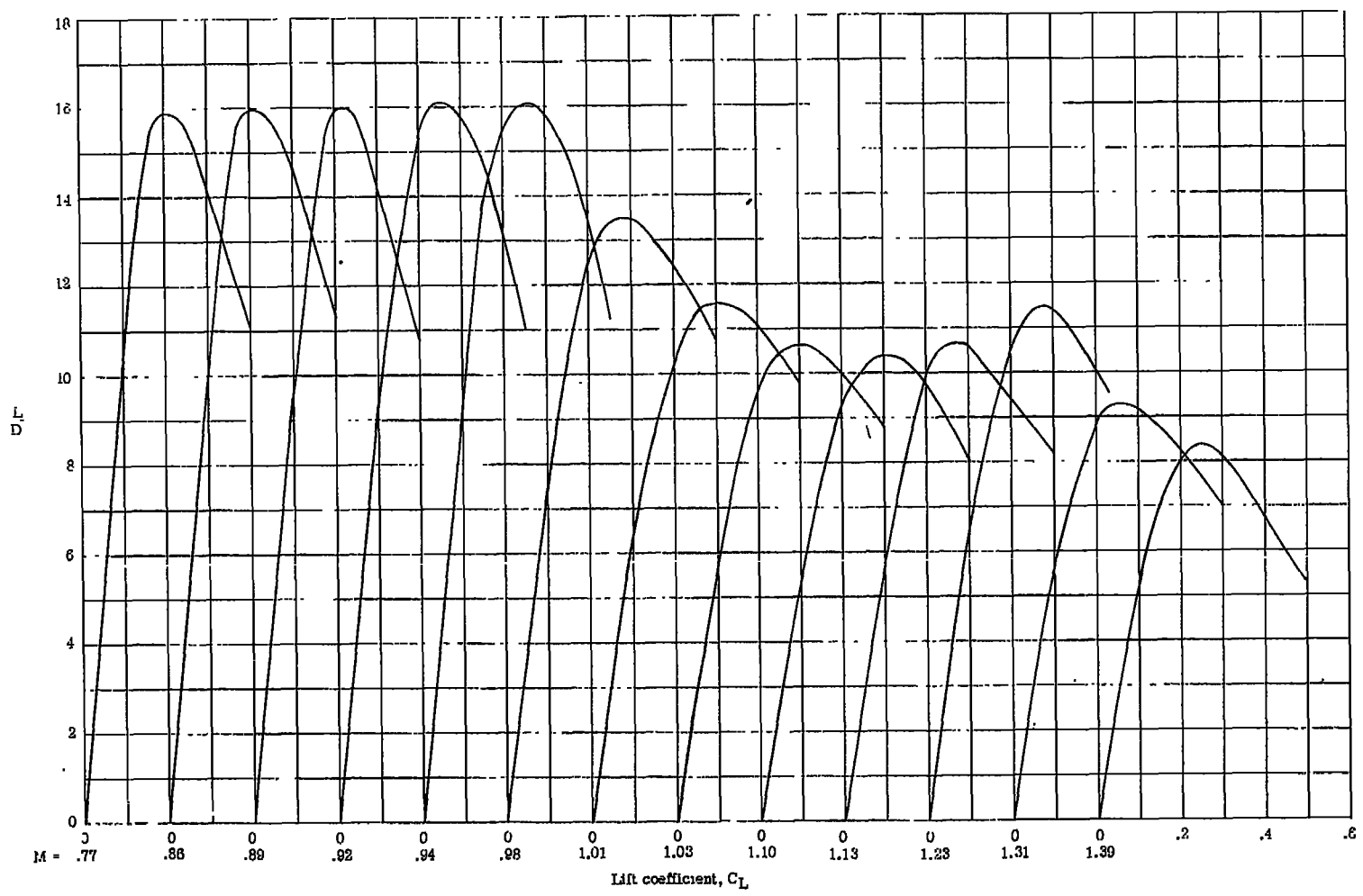


Figure 11.- Variation of lift-drag ratio with lift coefficient at various Mach numbers for the wing-body combination. Cambered and twisted delta wing; $\Lambda = 3$; $t/c = 0.03$.

CONFIDENTIAL

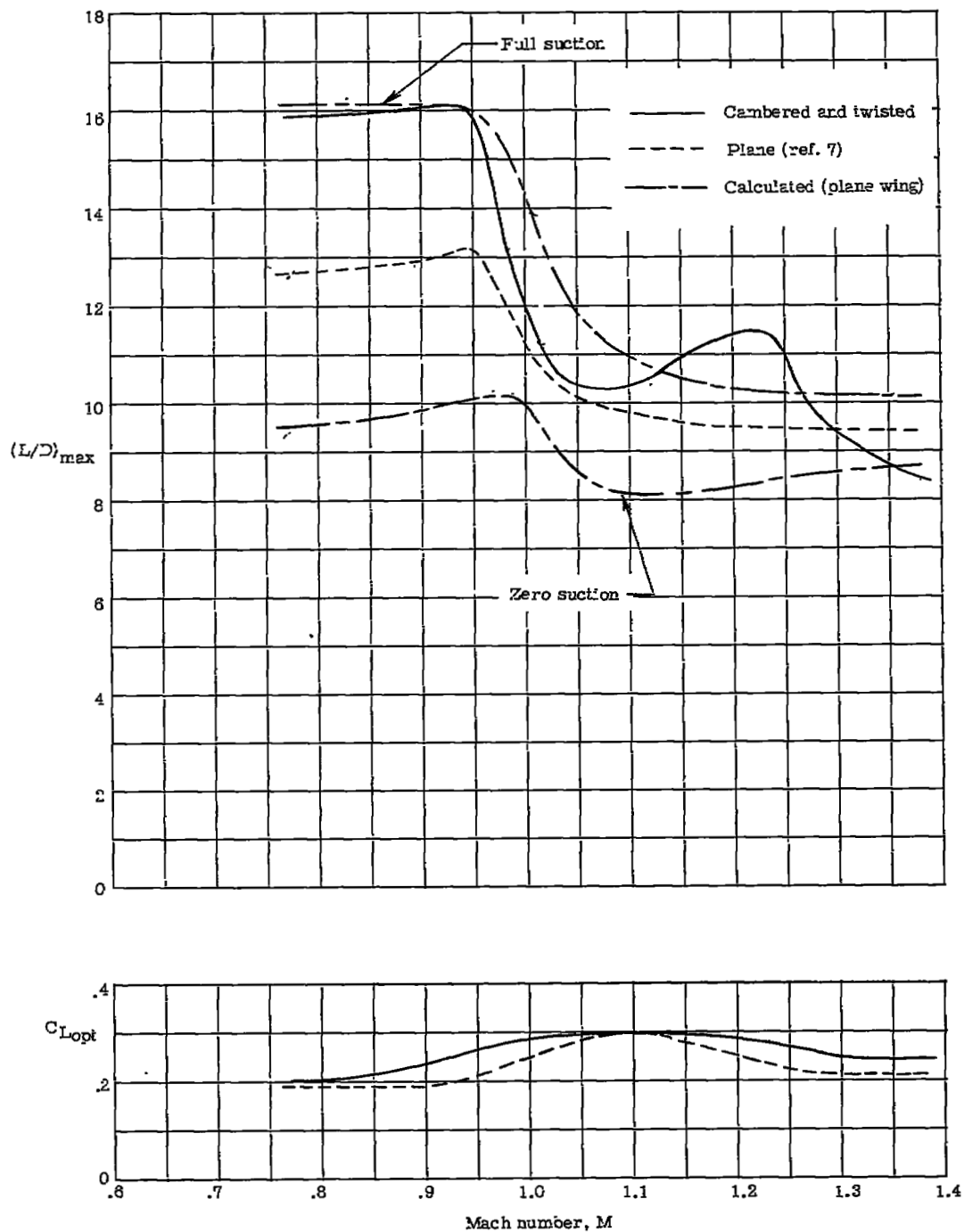


Figure 12.- Variation of $(L/D)_{max}$ and C_{Lopt} with Mach number for the wing-body combination. Delta wing; $A = 3$; $t/c = 0.03$.

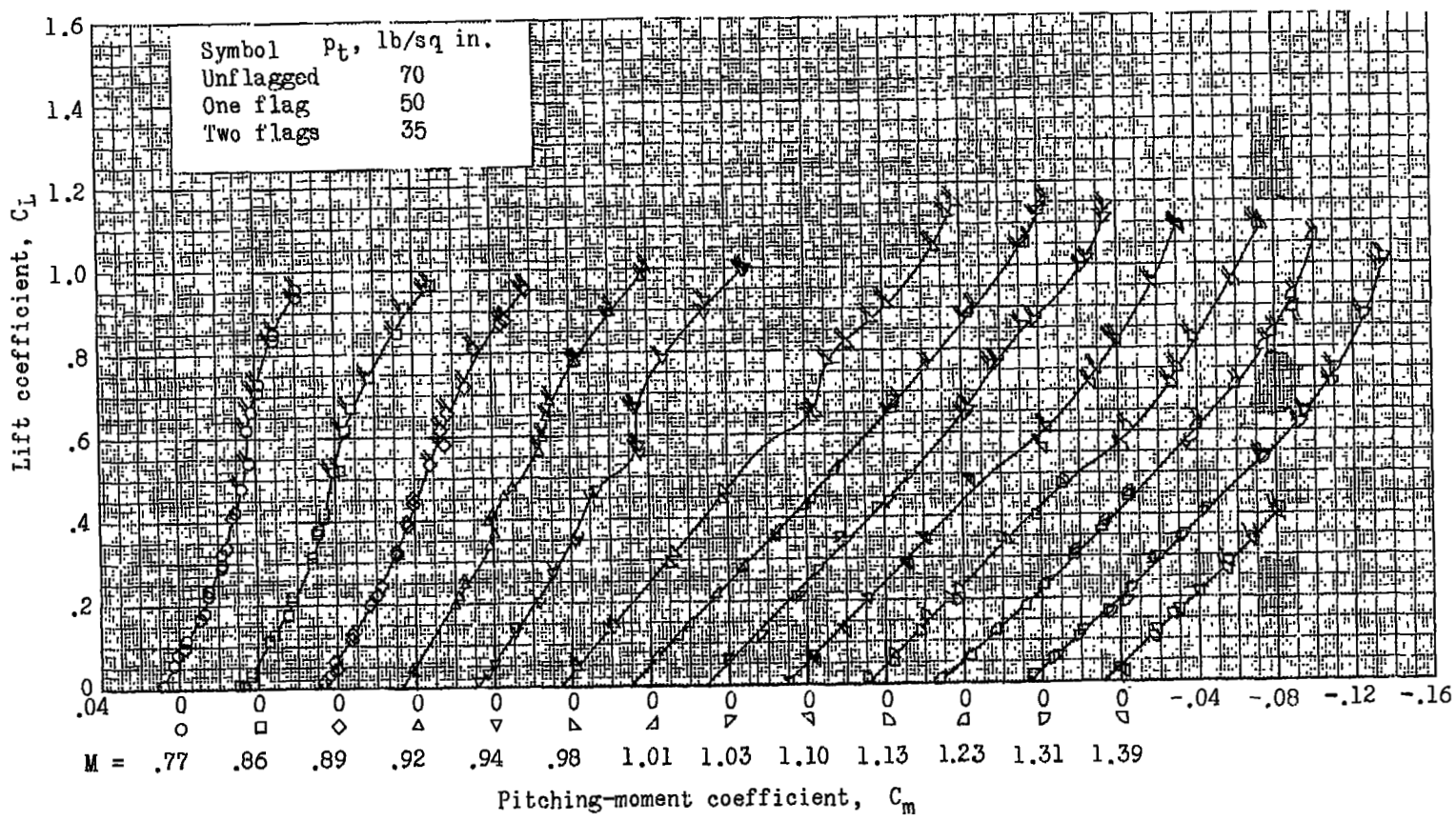


Figure 13.- Variation of lift coefficient with pitching-moment coefficient at various Mach numbers for the wing-body combination. Cambered and twisted wing; $A = 3$; $t/c = 0.03$.

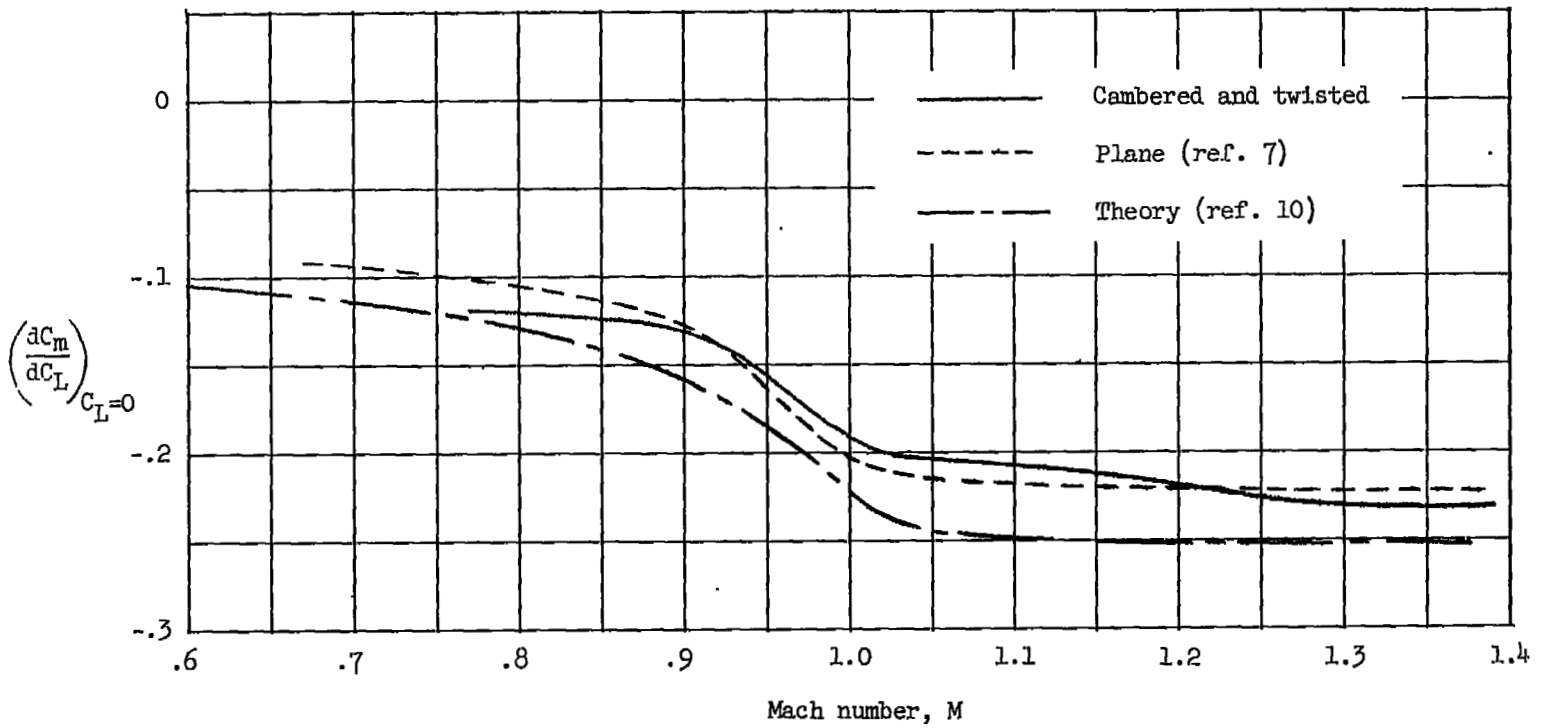


Figure 14.- Variation of pitching-moment lift-curve slope with Mach number for the wing-body combination. Delta wing; $A = 3$; $t/c = 0.03$.

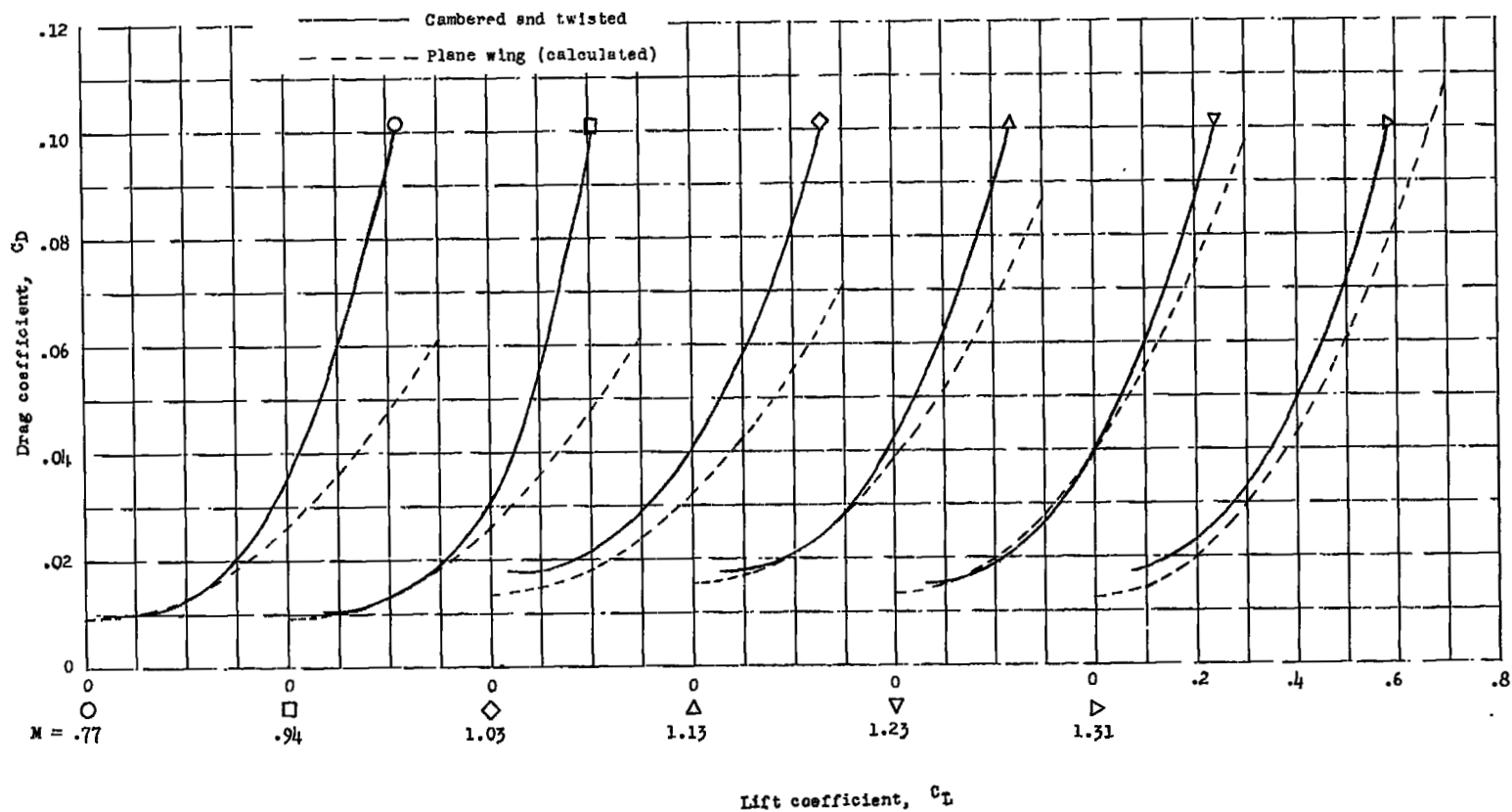


Figure 15.- A comparison of the lift-drag variation of the cambered and twisted wing at various Mach numbers with calculated minimum drag for lifting condition. Delta wing; $A = 3$; $t/c = 0.03$.

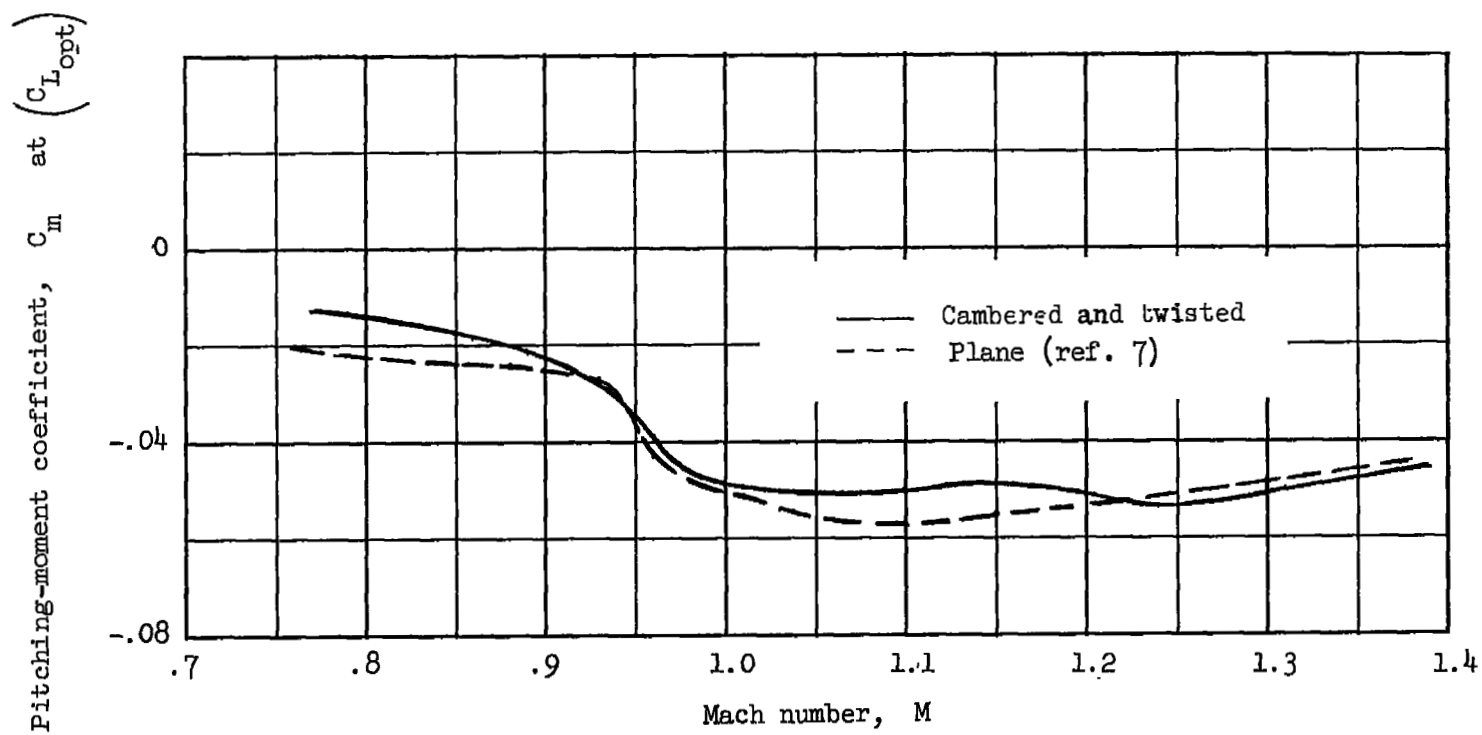


Figure 16.- Variation of pitching-moment coefficient at optimum lift with Mach number for the wing-body combination. Delta wing; $A = 3$; $t/c = 0.03$.

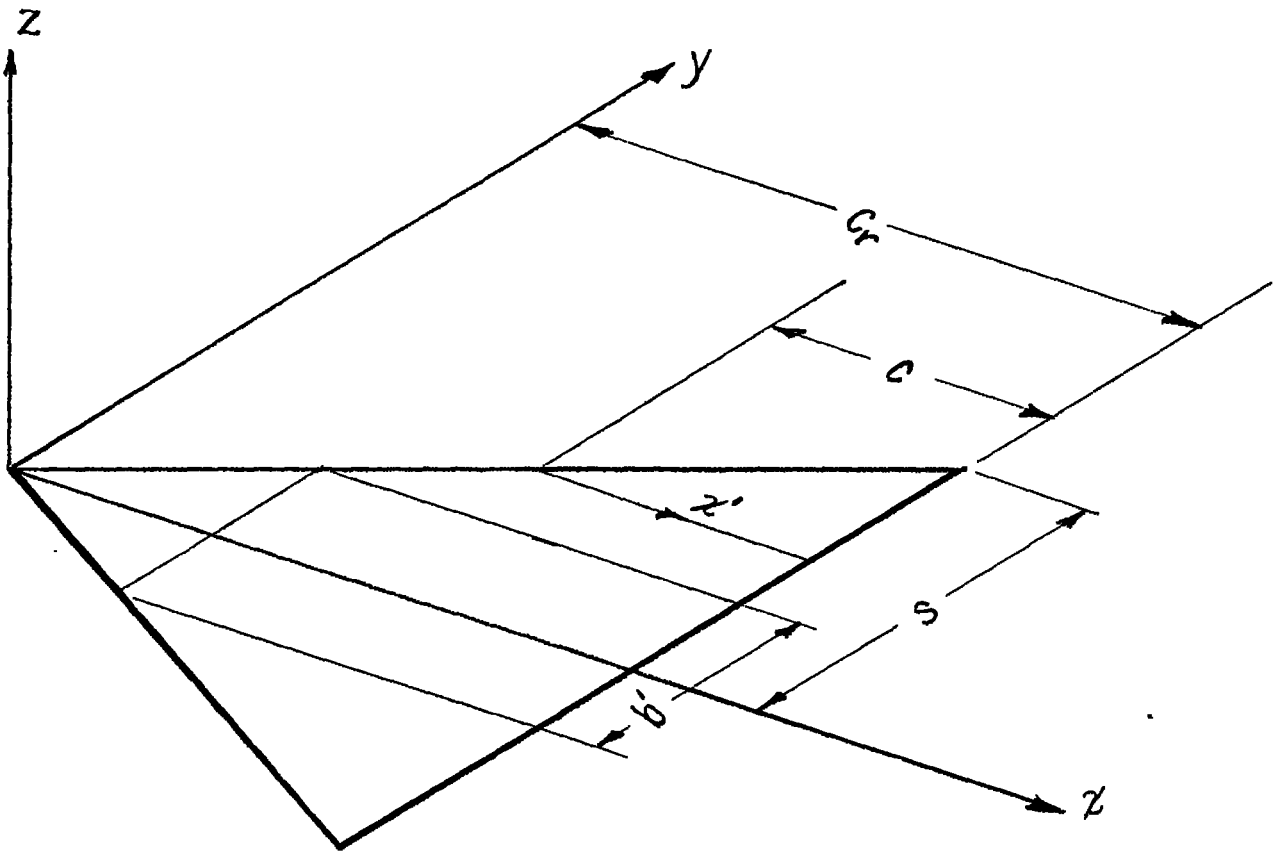


Figure 17.- Axis system for calculation of wing ordinates.



NASA Technical Library



3 1176 01438 0308

